DTIC FILE COPY

(1)

SECURITY CLASSIFICATION OF THIS PAGE

REPORT DOCUMENTATION PAGE

Form Approved OMB No 0704-0188

AD-A208 451

1b RESTRICTIVE MARKINGS: NONE

3 DISTRIBUTION/AVAILABILITY OF REPORT: APPROVED FOR PUBLIC RELEASE; DISTRIBUTION UNLIMITED.

4. PERFORMING ORGANIZATION REPORT NUMBER(S)

5. MONITORING ORGANIZATION REPORT NUMBER(S): AFIT/CI/CIA-88-202

6a. NAME OF PERFORMING ORGANIZATION: AFIT STUDENT AT Florida State University

6b. OFFICE SYMBOL (If applicable)

7a. NAME OF MONITORING ORGANIZATION: AFIT/CIA

6c. ADDRESS (City, State, and ZIP Code)

7b. ADDRESS (City, State, and ZIP Code): Wright-Patterson AFB OH 45433-6583

8a. NAME OF FUNDING/SPONSORING ORGANIZATION

8b. OFFICE SYMBOL (If applicable)

9. PROCUREMENT INSTRUMENT IDENTIFICATION NUMBER

8c. ADDRESS (City, State, and ZIP Code)

10. SOURCE OF FUNDING NUMBERS

PROGRAM ELEMENT NO.	PROJECT NO.	TASK NO	WORK UNIT ACCESSION NO.

11. TITLE (Include Security Classification) (UNCLASSIFIED) An Objective Comparison of Vertical Motions from the Kinematic Method and Three Forms of the Omega Equation

12. PERSONAL AUTHOR(S): Gerald Emil Hevrdeys

13a. TYPE OF REPORT	13b. TIME COVERED	14. DATE OF REPORT (Year, Month, Day)	15. PAGE COUNT
THESIS/DISSERTATION	FROM _____ TO _____	1988	96

16. SUPPLEMENTARY NOTATION: APPROVED FOR PUBLIC RELEASE IAW AFR 190-1
ERNEST A. HAYGOOD, 1st Lt, USAF
Executive Officer, Civilian Institution Programs

17. COSATI CODES		
FIELD	GROUP	SUB-GROUP

18. SUBJECT TERMS (Continue on reverse if necessary and identify by block number)

19. ABSTRACT (Continue on reverse if necessary and identify by block number)

20. DISTRIBUTION/AVAILABILITY OF ABSTRACT
☒ UNCLASSIFIED/UNLIMITED ☐ SAME AS RPT. ☐ DTIC USERS

21. ABSTRACT SECURITY CLASSIFICATION: UNCLASSIFIED

22a NAME OF RESPONSIBLE INDIVIDUAL	22b. TELEPHONE (Include Area Code)	22c. OFFICE SYMBOL
ERNEST A. HAYGOOD, 1st Lt, USAF	(513) 255-2259	AFIT/CI

DD Form 1473, JUN 86 — Previous editions are obsolete. — SECURITY CLASSIFICATION OF THIS PAGE

AFIT/CI "OVERPRINT"

THE FLORIDA STATE UNIVERSITY

COLLEGE OF ARTS AND SCIENCES

AN OBJECTIVE COMPARISON OF VERTICAL MOTIONS FROM THE KINEMATIC METHOD AND THREE FORMS OF THE OMEGA EQUATION

by

GERALD EMIL HEVRDEYS

A Thesis submitted to the
Department of Meteorology
in partial fulfillment of the
requirement for the degree of
Master of Science

Approved:

Henry E. Fuelberg
Professor Directing Thesis

Peter L. Lagasse

David W. Hyatt

Fall Semester, 1988

AN OBJECTIVE COMPARISON OF VERTICAL MOTIONS
FROM THE KINEMATIC METHOD AND THREE FORMS
OF THE OMEGA EQUATION

Gerald Emil Hevrdeys
The Florida State University, 1988

Major Professor: Henry E. Fuelberg, Ph.D.

Subjective and objective comparisons were performed on large scale vertical motions from the kinematic method, the traditional omega equation, Trenberth's form of the omega equation, and the Q vector approach. Vertical motions from these routines were qualitatively compared to flow patterns and cloud/precipitation regions associated with a developing midlatitude springtime cyclone during the period 17-19 March 1986. In addition, objective comparisons were accomplished using a scoring scheme which rated each method.

Results showed that kinematic motions were far superior to those from any of the three omega equation techniques. However, when the various omega equation output was compared with each other, they were found to be very similar. The Q vector method yielded slightly better scores for the entire 48 h period, but none of the three methods was clearly superior at the individual times. Because of the closeness of results, the omega equation

routines were judged according to their ease of use and computation. From this analysis, the Q vector algorithm was chosen as the best of the three methods.

ACKNOWLEDGEMENTS

I would like to thank Dr. Henry E. Fuelberg for his help in organizing and editing this thesis. In addition, I would also like to thank Dr. James T. Moore at St. Louis University for his help in deriving Trenberth's form of the omega equation. I would like to thank Ted Funk of NOAA/NESDIS at Washington D.C. for providing well documented computer programs which I used as guides for my own. The National Aeronautics and Space Administration provided support for this research under Grant NAG8-653 to Florida State University. The grant is under the auspices of the Remote Sensing Branch at Marshall Space Flight Center. The Air Force Institute of Technology, Civilian Institution Program provided funds and gave me the opportunity to attend school. Finally, special thanks to my wife Cheryl who assisted with the figures and provided moral support.

TABLE OF CONTENTS

LIST OF TABLES

LIST OF FIGURES

1. Introduction

The accurate calculation of vertical velocity on the synoptic scale is a definite challenge. Unlike other important meteorological parameters such as horizontal wind and temperature, synoptic scale vertical motion (ω = dp/dt) cannot be directly measured accurately. Therefore, it must be calculated indirectly from measured values. As with any calculations, the goodness of ω depends on the quality of the input data field, as well as the method used for its determination. Since representation of ω is almost a necessity for forecasting atmospheric processes such as cyclogenesis, convection, and precipitation, the best procedure of computing ω should be determined.

Miller and Panofsky (1958) and later Dutton (1976) described the kinematic, adiabatic, vorticity, precipitation, and quasi-geostrophic omega equation algorithms for obtaining vertical motion. Since each approach has its merits and limitations, the question arises as to which one provides the best results on the synoptic scale.

The kinematic method has been used in many studies, including Panofsky (1946), Bellamy (1949), Smith (1971), and Portis and Lamb (1988). The procedure is based on vertical integration of the continuity equation resulting

in (e.g., Dutton, 1976):

$$\omega(x,y,p) = \int_{p}^{p_o} \vec{\nabla}\cdot\vec{v}\ dp\,, \qquad (1)$$

where all symbols have their standard meanings and ω at the surface was assumed to be zero. Thus, ω can be found by vertically integrating the horizontal divergence at various pressure levels.

The only major assumption of the kinematic approach is that the atmosphere is hydrostatic, which is reasonable on the synoptic scale. An advantage of the procedure is the relative ease of calculation, i.e., wind data from the routine rawinsonde network can be readily inserted into (1). A disadvantage is that rawinsonde-derived winds possess increasing error with height. As Belt and Fuelberg (1982) have shown, these errors can have a significant impact on ω, because even small wind errors will cause large errors in the derived divergence, and thus large errors in ω, especially in the upper troposphere. For this reason, it is necessary to correct the derived vertical motion. O'Brien (1970) has shown that a much more realistic vertical profile of ω is achieved by setting the boundary conditions to zero and then applying a weighted correction to the original estimates.

The adiabatic method attempts to calculate vertical motion by the following expression derived from the

thermodynamic energy equation (Dutton, 1976):

$$\omega = - \frac{\left(\partial T/\partial t\right) + \vec{v} \cdot \vec{\nabla}_p T}{\left(\partial T/\partial p\right) - \left(g/c_p\right)}, \qquad (2)$$

where C_p is the specific heat of dry air at constant pressure. Vertical motion in (2) depends on three expressions: the local change of temperature with time, the advection of temperature on a constant pressure surface, and the environmental lapse rate.

An advantage of the adiabatic technique is that rawinsonde-derived temperature data are more accurate than wind data (Belt and Fuelberg, 1982). Thus, by using thermal data instead of wind data to calculate ω, the problem of wind error with the kinematic method is reduced. Nevertheless, the adiabatic procedure does have several limitations. First, since rawinsonde soundings are only available every 12 h, the time derivative in (2) can cause errors in ω. Errors will also occur when the lapse rate approaches adiabatic, which causes the above equation to become unbounded. Another important point is that diabatic processes are neglected under the basic assumptions used to obtain (2). These disadvantages are the reason the adiabatic method is less popular than most other ways of computing ω. Miller and Panofsky (1958), Wilson (1976), Fuelberg and Lee (1982) have objectively compared the adiabatic method to the kinematic procedure and have

shown that the kinematic technique yields the more realistic patterns and values for ω when compared with cloud and precipitation patterns.

The vorticity method is based on a simplified form of the vorticity equation that yields (Dutton, 1976):

$$\omega(p) = (\zeta_p + f)\int_0^p \frac{1}{(\zeta_p+f)^2}\left(\frac{\partial}{\partial t} + \vec{v}\cdot\vec{\nabla}_p\right)(\zeta_p+f)\,dp, \qquad (3)$$

where ζ_p is relative vorticity on a constant pressure surface and f is the Coriolis parameter. Vertical motion at the surface is assumed to be zero. There are two major expressions which control the values of ω, the local change in absolute vorticity and the advection of absolute vorticity on constant pressure surfaces. By calculating these expressions at various levels and then integrating, a vertical profile for ω is found.

The approach has several disadvantages. As with the adiabatic version, the infrequency of rawinsonde data can cause significant errors in the local time derivative. In addition, the tendency for the local derivative and advection terms to cancel each other is another problem because ω then results from a small difference in two larger terms. Finally, the twisting or tilting terms were omitted from (3) for simplification purposes. On the synoptic scale, these two terms are normally small compared to the time change and advection terms, but their

omission could reduce the accuracy of ω in some situations.

The precipitation method (Bannon, 1948) is based on an assumed relationship between vertical motion and rainfall using the following expression:

$$\omega = -\frac{P}{\int \left[\Gamma_m \left(\frac{r}{T} + \frac{\partial r}{\partial T} \right) - \frac{gr}{RT} \right] dz} , \qquad (4)$$

where P is the measured precipitation rate, Γ_m is the saturated adiabatic lapse rate, R is the gas constant, and r is the mixing ratio. Specifically, this routine assumes that upward vertical motion occurs at the same time and place as precipitation. Of course, this may not be true for a variety of reasons. Another disadvantage is the difficulty in measuring precipitation on the synoptic scale. The distance between reporting stations causes convective precipitation to be especially poorly sampled. This procedure is rarely used because of its limitations.

More recent techniques for calculating ω use variations of the quasi-geostrophic omega equation. The following expression is the traditional version of that formula (Holton, 1979):

$$\left(\nabla^2 \sigma + f_o^2 \frac{\partial^2}{\partial p^2} \right) \omega = f_o \frac{\partial}{\partial p} \left[\vec{V}_g \cdot \vec{\nabla} \left(\frac{1}{f_o} \nabla^2 \Phi + f \right) \right] + \nabla^2 \left[\vec{V}_g \cdot \vec{\nabla} \left(-\frac{\partial \Phi}{\partial p} \right) \right] , \qquad (5)$$

where σ is the static stability parameter, f_o is a con-

stant value of the Coriolis parameter, and Φ is geopotential height. The formula is derived by combining the adiabatic form of the thermodynamic energy equation with the quasi-geostrophic vorticity equation. Due to the simplifying assumptions of these equations, (5) also is valid only for large scale flows. Vertical motion is determined by the two forcing functions on the right hand side of the expression. The first term describes differential vorticity advection in the vertical, while the second is the horizontal Laplacian of thickness advection. Thus, upward motion is associated with upward increasing positive vorticity advection and localized maxima of positive thickness advection.

An advantage of (5) is that it is a diagnostic equation, thereby eliminating the problems with time derivatives inherent in both the adiabatic and vorticity methods. Another advantage is the use of geostrophic winds instead of observed winds. This reduces the problem of the more inaccurate rawinsonde-derived winds that occurred with the kinematic method. A disadvantage is that the algorithm requires more computational time than the earlier procedures. This occurs because the differential vorticity advection term tends to be weaker in the lower layers than the thickness advection term, while stronger in the upper layers. For this reason, three-dimensional relaxation must be accomplished to get a representative

profile for ω. In addition, the two forcing functions can cancel each other as they did in the vorticity method, thereby leading to increased uncertainty. The final disadvantage is the adiabatic assumption which is violated near the surface and in regions of clouds and precipitation.

To overcome the problem of term cancellation in the traditional omega equation, Trenberth (1978) proposed a rederived version based on the work of Sutcliffe (1947):

$$\left(\nabla^2\sigma + f_o^2\frac{\partial^2}{\partial p^2}\right)\omega = 2f_o\left(\frac{\partial \vec{V}_g}{\partial p}\right)\cdot\vec{\nabla}\zeta_g - \frac{2R}{pf_o}\left[J\left(u,\frac{\partial T}{\partial y}\right) - J\left(v,\frac{\partial T}{\partial x}\right)\right], \quad (6)$$

where ζ_g is geostrophic vorticity and J is the Jacobian. The terms on the right hand side of (6) represent advection of vorticity by the thermal wind and a deformation function. In developing this equation, the difference between relative vorticity and absolute vorticity was ignored in the first term; however, this causes minimal loss in accuracy (Durran and Snellman, 1987). The deformation term usually is small compared to the advection term in the middle troposphere (about 700 to 350 mb) and outside of frontal zones. If deformation is neglected, the right hand side reduces to a single forcing function. Thus, upward motion occurs in regions where there is cyclonic vorticity advection by the thermal wind.

Hoskins et al. (1978) also rederived the traditional

omega equation to yield the following expression:

$$\left(\nabla^2\sigma + f_o^2\frac{\partial^2}{\partial p^2}\right)\omega = -2\vec{\nabla}\cdot\vec{Q} \quad , \tag{7}$$

where

$$\vec{Q} = \left[-\left(\frac{g}{\theta_o}\right)\left(\frac{\partial\vec{V}_g}{\partial x}\right)\cdot\vec{\nabla}\theta \quad , \quad -\left(\frac{g}{\theta_o}\right)\left(\frac{\partial\vec{V}_g}{\partial y}\right)\cdot\vec{\nabla}\theta\right] . \tag{8}$$

In this formulation, the two original forcing functions in (5) are again reduced to one, the divergence of "Q vectors". The Q vector is the ageostrophic horizontal wind that forms in the lower layers to maintain thermal wind balance (Hoskins and Pedder, 1980). Barnes (1985) used an equation similar to Hoskins et al. (1978), except he defined the Q vector as:

$$\vec{Q} = \left[-\frac{\partial\vec{V}_g}{\partial x}\cdot\vec{\nabla}\left(-\frac{\partial\Phi}{\partial p}\right) \quad , \quad -\frac{\partial\vec{V}_g}{\partial y}\cdot\nabla\left(-\frac{\partial\Phi}{\partial p}\right)\right] . \tag{9}$$

Barnes' expression uses thickness instead of potential temperature to calculate Q vectors; however, the forms are equivalent.

An advantage of the Q vector method is that vertical motion at a given level can be implied from the convergence/divergence of the Q vectors at that particular level (Durran and Snellman, 1987). Where Q vectors diverge, downward vertical motion is implied, while upward vertical

motion is associated with converging Q vectors. Barnes (1986) found that the best Q vector ω fields were produced well within the boundaries of the data region, and when only synoptic scale data resolution was sought. Since the data were heavily filtered, some small scale features were missed. Another advantage is that unlike the expression suggested by Trenberth (1978), the Q vector approach does not neglect any processes, e.g., deformation. Thus, it is equivalent to the traditional omega equation and should be more applicable to the actual environment.

Vertical motion fields calculated from the Q vector technique will differ from those produced by the traditional and Trenberth methods since different finite differencing forms are used. In addition, Durran and Snellman (1987) noted that each forcing function on the right hand side of the traditional method (5) contains the term advection of thermal vorticity by the wind. These terms cancel exactly in continuous expressions, but only approximately in the finite difference forms used in calculations. They noted that the problem is especially pronounced when there is poor numerical resolution, especially in the vertical. This cancellation problem does not occur in Trenberth's version or the Q vector approach. In fact, Durran and Snellman (1987) speculated that Trenberth's version, even after neglecting deformation,

may yield better results than the exact, traditional form (5) in certain conditions. One of the goals of this investigation is to assess the differences in quasi-geostrophic ω that result from these numerical considerations.

Determining which scheme for obtaining ω produces the best results has been the focus of several studies. Smith (1971), Vincent et al. (1976), and Smith and Lin (1978) have compared the traditional form of the omega equation with the kinematic method. Recently, Blakley et al. (1986) and Durran and Snellman (1987) have subjectively compared the Q vector approach with other procedures. Results from of all these studies showed that ω fields produced by the modified omega equations correlated well with precipitation regions; however, the kinematic method still yielded the best agreements.

The purpose of this paper is to provide an objective comparison between the kinematic method, the traditional quasi-geostrophic omega equation, Trenberth's omega equation, and Barnes' Q vector approach. A scoring scheme will be used to relate cloud cover and precipitation with calculated fields of ω. The case being studied contains a developing springtime cyclone with pronounced forcing and well defined areas of clouds and clear skies.

2. Data and methodology

The area of study covered most of the continental United States along with parts of northern Mexico. Data for the period 17-19 March 1986 came from two primary sources, rawinsonde soundings archived by the National Climatic Data Center, and facsimile charts from the National Weather Service. Soundings from 65 rawinsonde stations were used over the area, with 12 h intervals between launches. The rawinsonde data were at 50 mb increments from the surface to 50 mb. Values of height, temperature, and u and v wind components were available. All data were checked for accuracy, with missing data replaced with values obtained from subjective analyses of the fields. This procedure was only necessary in the upper levels where strong jet stream winds led to early termination of some soundings.

Facsimile charts prepared by the National Weather Service included analyses at the surface, 850 mb, 700 mb, 500 mb, and 300 mb, as well as radar summaries. Surface charts were hand analyzed for cloud cover and precipitation locations.

Rawinsonde data were the only input used to calculate vertical motions from each of the four methods. The data

were first placed on a 27x18 grid (Fig. 1) so that centered finite differencing techniques could be used to evaluate the partial derivatives in the various schemes. Station values of height, temperature, and u and v wind components were interpolated onto the 158 km grid using the Barnes (1973) objective analysis technique. Since this study was concerned with large scale vertical motions, the chosen response was 14% of 800 km wavelengths (twice the average sounding spacing). This strong filtering limited the size of the vertical motion patterns to only synoptic scale features. The kinematic vertical motions were originally calculated with a 46% response at 800 km, which is consistent with previous studies such as Fuelberg and Funk (1987). However, the omega equation procedures are based on quasi-geostrophic concepts which are only applicable to the large scales, i.e., a much smaller response. Trial calculations of the traditional omega equation were made at 8%, 14%, 20%, and 28% responses, with very similar results for each. The 14% response was chosen for final calculations since Barnes (1986) cautions against the use of gridded data containing mesoscale features because they would lead to unrealistic patterns of Q vectors. Thus, for fairness in the scoring procedure, data from a 14% response was used for all four methods.

Kinematic vertical motions were calculated using (1),

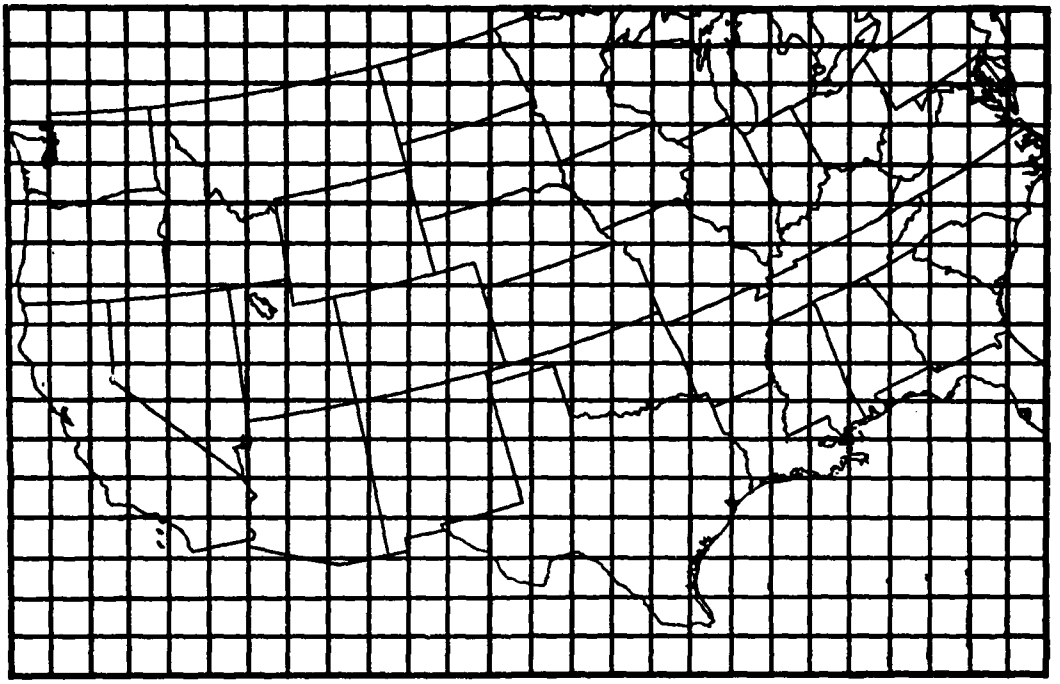

Fig. 1 Grid used for finite differencing.

giving fields of ω every 50 mb from the surface to 50 mb. The O'Brien (1970) adjustment scheme was then used on the results to give more realistic profiles of ω. The vertical motion at 50 mb was set to zero, with the weighted correction applied to the rest of the profile being a linear function of the pressure. Specifically, there is no correction at the surface where vertical motion is assumed to be zero, while the maximum adjustment is at 50 mb where the vertical motion is forced back to zero.

Before calculating vertical motions from the three omega equation routines, geostrophic winds were obtained from the rawinsonde-derived heights. The stability parameter σ was calculated at each time, and was assumed to vary with height, but be constant on each pressure surface. The traditional omega equation was used in the form shown in (5). First, the two forcing functions on the right hand side of the expression were obtained. Then, three-dimensional relaxation (Haltiner and Williams, 1980) was used on each term separately, employing a residual of 0.005 microbars/s. Boundary conditions of $\omega = 0$ were employed at 1000 mb (bottom), 50 mb (top), and all lateral sides. The two components were then added together to obtain the total vertical motion at 50 mb intervals.

Vertical motions from Trenberth's procedure (6) were obtained by relaxing its forcing functions, using the same

residual as before. Although the deformation term in (6) is usually neglected, current vertical motions were calculated both with and without it. Results for the March 1986 case were very similar, with vertical motions differing only 0.1 to 0.5 microbars/s at 700 mb and 500 mb. For the sake of completeness, the scoring of Trenberth's formulation was accomplished both with and without the deformation function.

The final modified omega equation method used (7) to calculate vertical motion from Q vectors in the form of (9) as proposed by Barnes (1985). Once again the forcing function on the right hand side was relaxed with the same residual as before.

3. Synoptic conditions

The synoptic case investigated in this study had a variety of features. The period involved a developing midlatitude springtime cyclone sampled during a 48 h period. As the cyclone matured, overcast and cloudfree areas near the frontal zone became more defined. Strong regions of rising motion and subsidence were assumed to be present because of these well defined cloud patterns. Precipitation types around the cyclone ranged from snow to thunderstorms. The snow was behind the main low, in a type of wrap-around configuration. These associated vertical motions were assumed to be difficult to detect, thereby providing a good test for each method. The thunderstorms occurring along the front were severe at times.

Figure 2 shows the surface and 500 mb synoptic situation at 1200 GMT 17 March 1986. Scalloping denotes lower and middle layer ceilings. A low pressure center was forming over southeast Colorado at the triple point of an occluding cyclone. Cloud cover was situated primarily over the old low in northern Wyoming and ahead of the occluded and warm fronts. There was also an area of cloudiness over much of southern California and Arizona.

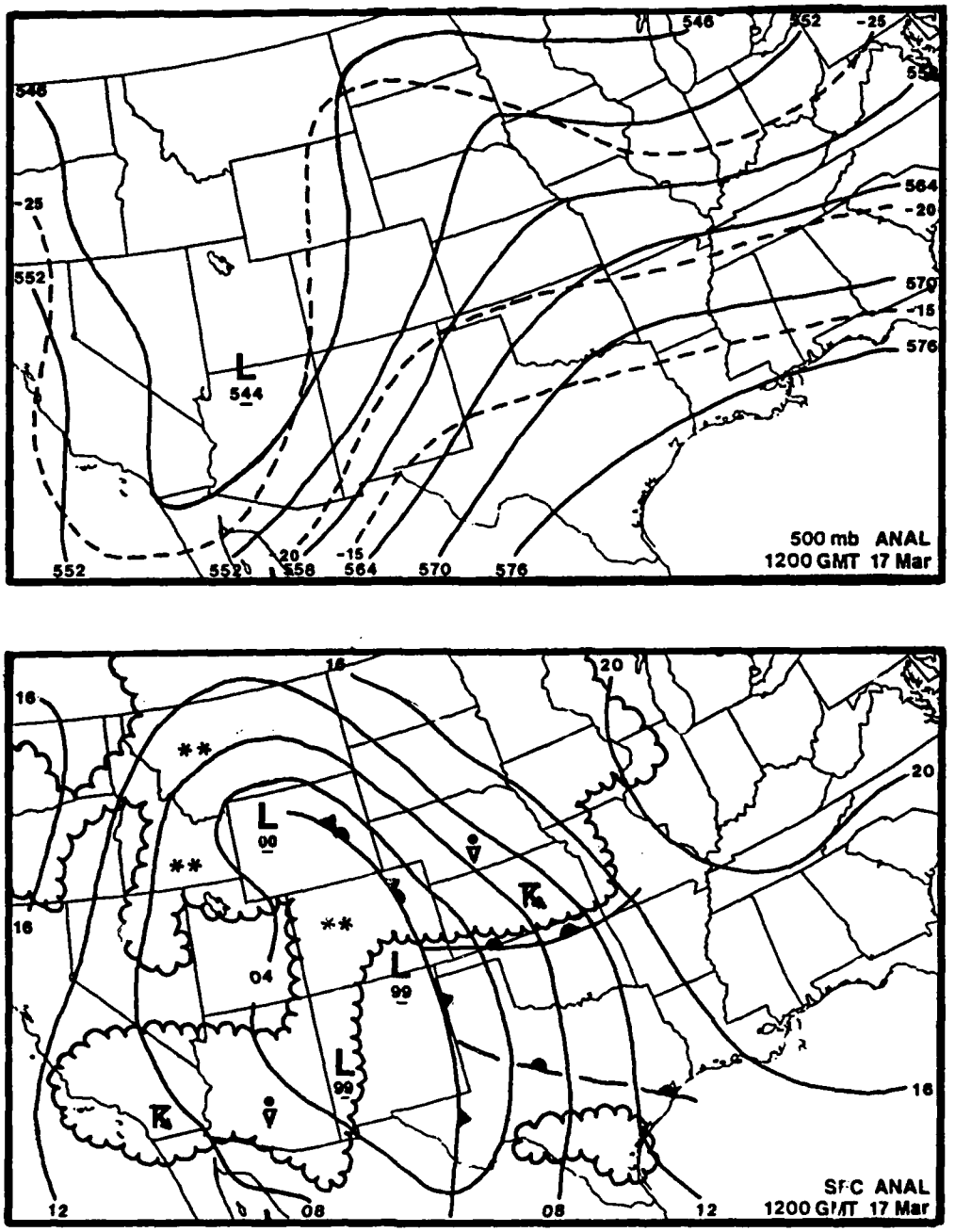

Fig. 2 Surface and 500 mb analyses for 1200 GMT 17 March 1986. At the surface, scalloped areas denote low and middle cloud ceilings that are either broken or overcast. At 500 mb, solid lines are height contours in decameters while dashed lines are isotherms in °C.

Precipitation at this time fell in three areas: a band of snow from Montana to northern Utah around the old low, showers and weak thunderstorms in Kansas and Nebraska associated with the warm front, and another area of weak showers and thunderstorms in southern California caused by an upper level trough.

A major upper level trough was present at 500 mb (Fig. 2). Its center was located in northern Arizona. Strongest winds at this level (not shown) stretched from Baja, Mexico to Dodge City, KS with a maximum of 80 kts over El Paso, TX. This jet streak provided good upper level support to the developing low in its left front quadrant. In addition, the isotherm pattern indicates cold air advection over the surface low.

By 0000 GMT 18 March 1986 (Fig. 3), the cyclone had developed into a traditional open wave with a second low trailing behind. The primary low pressure center had moved into southwestern Kansas and deepened from 999 to 992 mb. The trailing low deepened from 999 to 994 mb as it moved across New Mexico during the past 12 h. The cloud pattern at 0000 GMT began to resemble a comma shape, as it wrapped around the new low. As would be expected, stratocumulus clouds were ahead of the warm front becoming stratus clouds behind the low, while cumulus clouds appeared ahead of the cold front. The area between the cold front and the surface trough over New Mexico con-

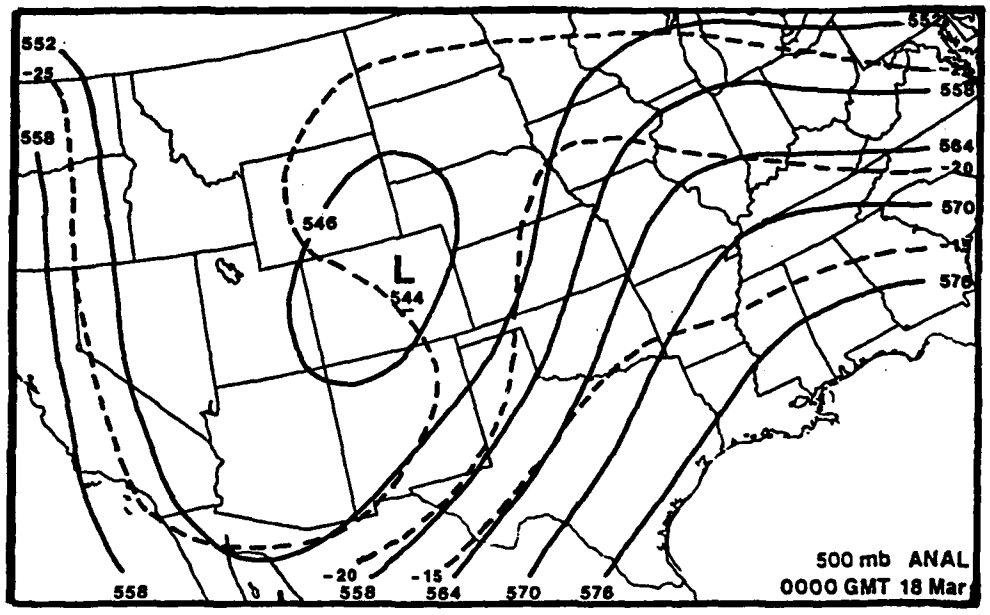

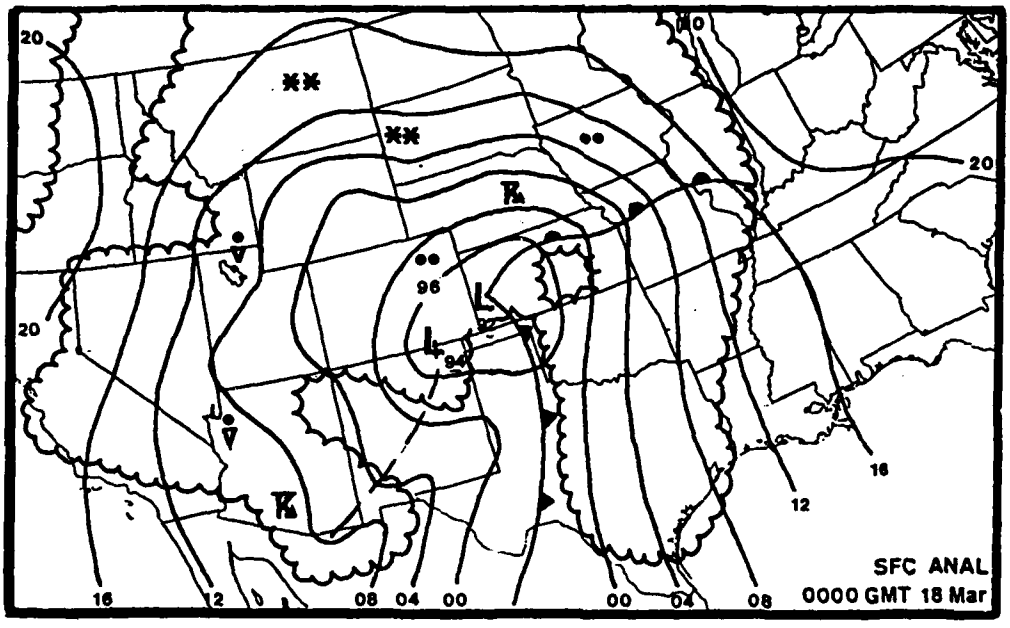

Fig. 3 As in Fig. 2, but for 0000 GMT 18 March 1986.

tained only scattered clouds which suggested subsidence. Precipitation was widely scattered, with most of the thunderstorm activity ahead of the warm front. Four hours prior to this time, radar summaries showed strong thunderstorms with hail in southcentral Nebraska. Light rain was widespread to the north and west of the main low center, but it changed to snow farther north. Some showers and weak thunderstorms were still lingering behind the secondary trough in southern California and Arizona. Only light rain had occurred ahead of the cold front up to this time.

At 500 mb (Fig. 3), the low center had not deepened further in the past 12 h; however, the trough axis had moved eastward, and the low had become broader. The jet axis (not shown) was now from Chihuahua, Mexico to Topeka, KS with a maximum of 90 kts over Del Rio, TX. One should notice the diffluent area over Nebraska which helped form the severe thunderstorms in that area. Cold air continued to advect into the leading side of the 500 mb trough.

Surface features at 1200 GMT 18 March 1986 (Fig. 4) were much more dramatic than those seen earlier. The two low centers had combined and moved to the northeast, while the cloud shield around the cyclone now was comma shaped with the trailing trough outlining the edge of the wrap-around stratus. Some clouds lingered behind the cold front, but there was still a definite clear area between

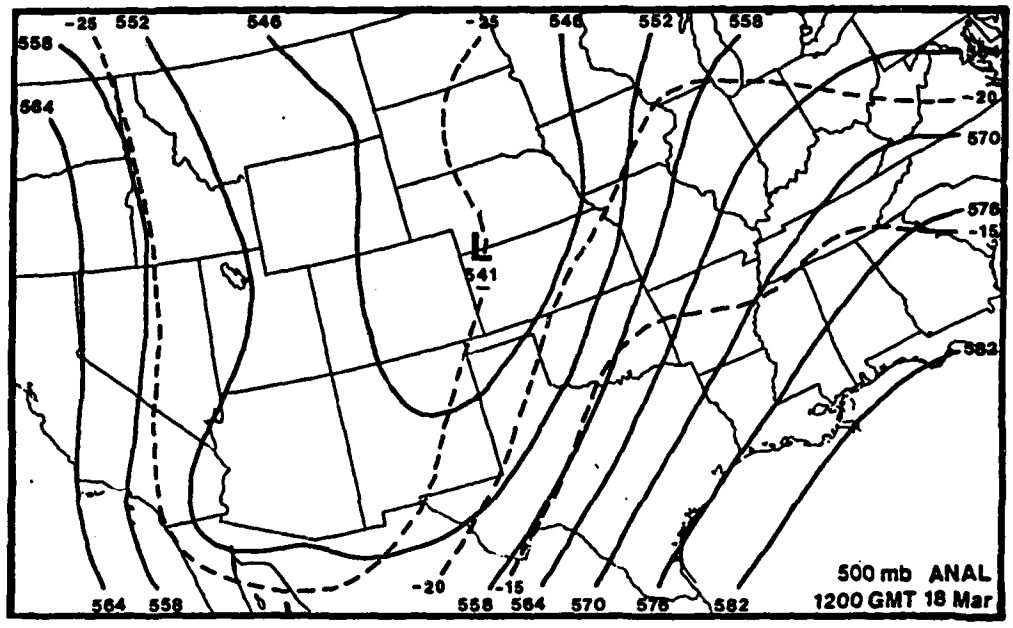

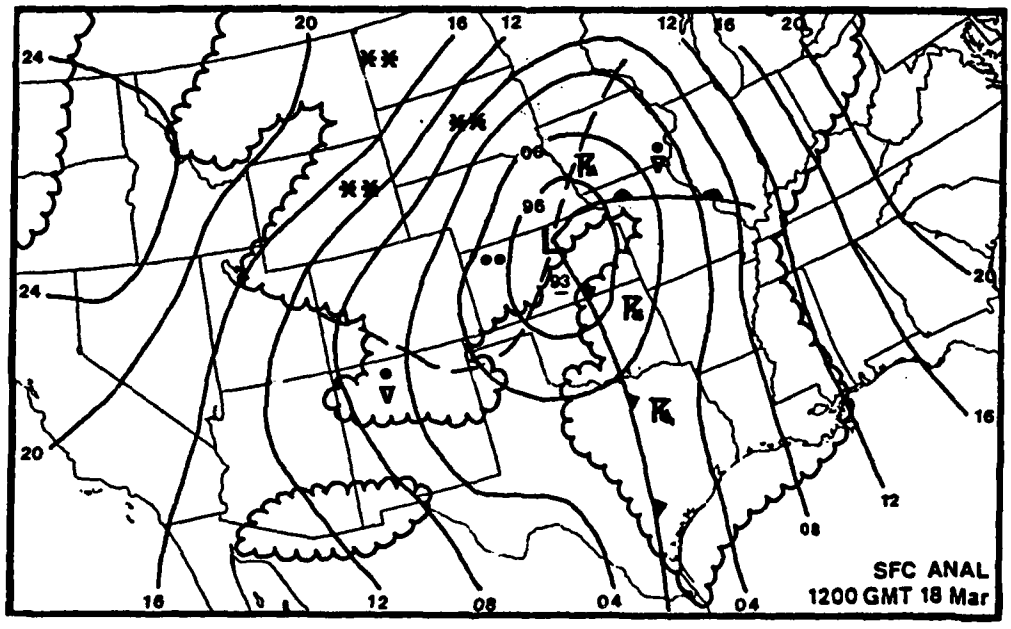

Fig. 4 As in Fig. 2, but for 1200 GMT 18 March 1986.

the front and surface trough. Precipitation had become stronger over the past 12 h, especially ahead of the cold front. Thunderstorms had developed along the cold front, while the area ahead of the warm front continued having rain and thundershowers. Snow was falling through most of the Dakotas, Montana, Wyoming and Colorado, but changed to rainshowers in northern New Mexico.

At 500 mb (Fig. 4), the low had deepened from 5440 to 5410 m over the past 12 h. The bulge over southern California suggested that the wave over the central United States had split from the main trough over the Rockies. The jet axis (not shown) extended from Del Rio, TX to Topeka, KS with a maximum of 100 kts over Oklahoma City, OK. Cold air advection had become less pronounced ahead of the 500 mb trough.

By the final time, 0000 GMT 19 March 1986 (Fig. 5), the surface cyclone had intensified further and moved into Iowa. The central pressure had dropped 5 mb over the past 12 h, and clouds almost surrounded the cyclone, with the exception of a clear wedge between the cold front and its trailing trough. Some clouds were also present over Montana and Wyoming in association with another trough. Precipitation over the past 6 h was intense, with severe thunderstorms developing along the entire cold front, as well as ahead of the warm front. Several squall lines had formed through Louisiana, Arkansas, and Mississippi, and

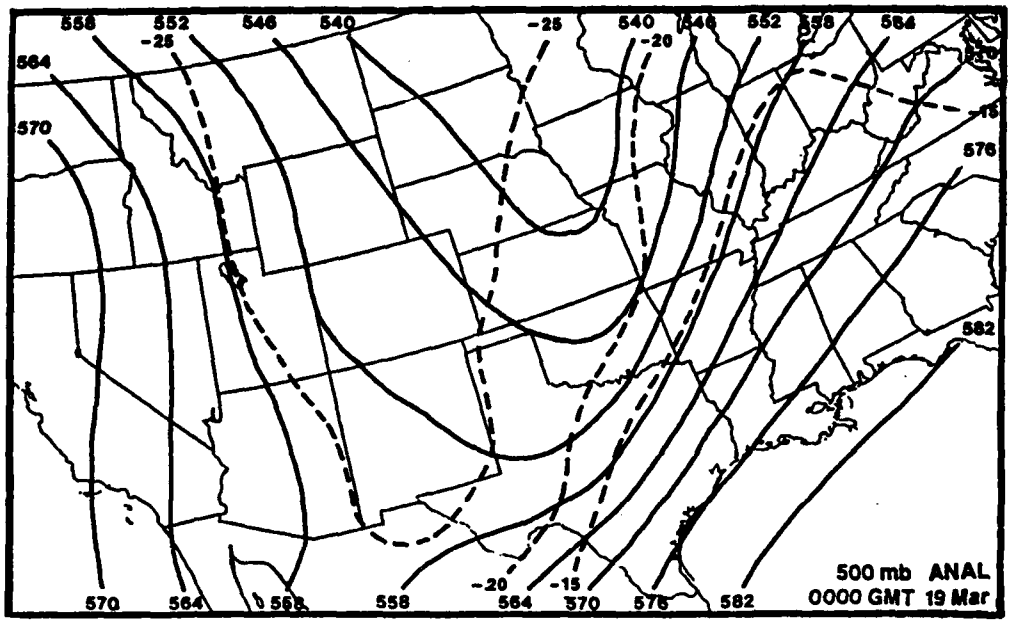

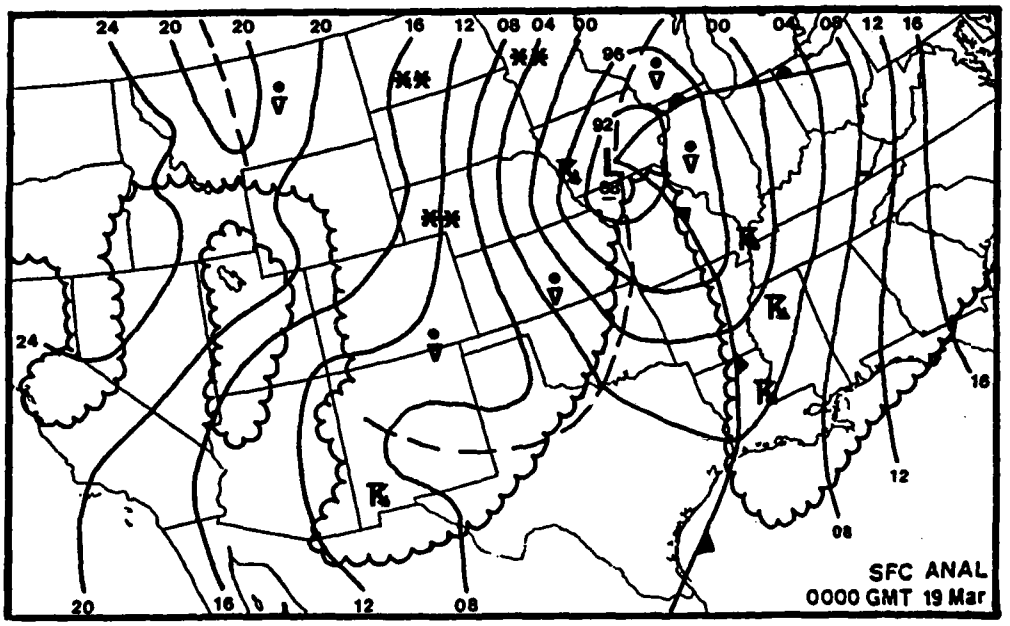

Fig. 5 As in Fig. 2, but for 0000 GMT 19 March 1986.

radar summaries also indicated hail in southwestern Iowa. Some weaker thunderstorms were also reported in New Mexico along the trailing trough. Snow continued to fall through the Dakotas and Minnesota, while some showers were present near the trough in Montana.

At 500 mb (Fig. 5), the trough axis continued to move eastward, becoming negatively tilted which suggested weakening. However, the winds (not shown) remained strong with the jet stream from Laredo, TX to Detroit, MI having a maximum of 115 kts over Dallas, TX. There now was little temperature advection ahead of the 500 mb trough.

4. Results

a. Subjective comparisons

Before presenting objective evaluations of the various methods, the computed vertical motion fields will be subjectively compared to each other and to the synoptic conditions. The basic assumption for comparison is that sustained upward vertical motion leads to clouds and precipitation, while downward motion leads to fair conditions. It is important to look at ω on a broad scale so its overall configuration can be seen in relation to flow patterns and cloud and precipitation regions. On the other hand, some features in the cloud patterns (Figs. 2-5) are smaller than was resolved by the objectively analyzed data (i.e., 14% of 800 km wavelengths). Thus, these cloud features may not agree with the vertical motion patterns.

Fuelberg and Lee (1982) emphasized several important points when relating clouds/precipitation to vertical motion. First, clouds may form without significant synoptic scale upward motion. For example, clouds may result from mixing or other small scale phenomena. Also,

even weak upward motion can produce strong convection if the environment is sufficiently unstable. In addition, an area may experience upward motion for several hours before clouds and precipitation form. Finally, areas of maximum ascent do not always align with areas of maximum cloud cover or precipitation. These aspects are important when considering the results that follow.

The kinematic method is the first routine to be analyzed. Figure 6 shows calculated ω fields at 1200 GMT 17 March for 700 mb and 500 mb. Values are given in microbars/s; however, a rough conversion for this case is that 1 microbar/s equals 1 cm/s at 700 mb and 1.25 cm/s at 500 mb. The overall ω pattern at 700 mb corresponds very well to the surface features (Fig. 2). For example, the area of strongest ascent (negative values) is ahead of the warm front over western Nebraska and Kansas, where thunderstorms and rain were reported. In general, most clouds and precipitation occur in areas of rising motion. An exception is a thunderstorm over San Diego, CA; however, this area is close to the data boundary where results are not expected to be as reliable as in the interior. Also note the weak subsidence over New Mexico, which corresponds to a clear slot behind the cold front. Magnitudes of ω at 700 mb generally are less than 2 microbars/s, but maximum values at 500 mb are over 4 microbars/s. At 500 mb, the maximum upward motion is over

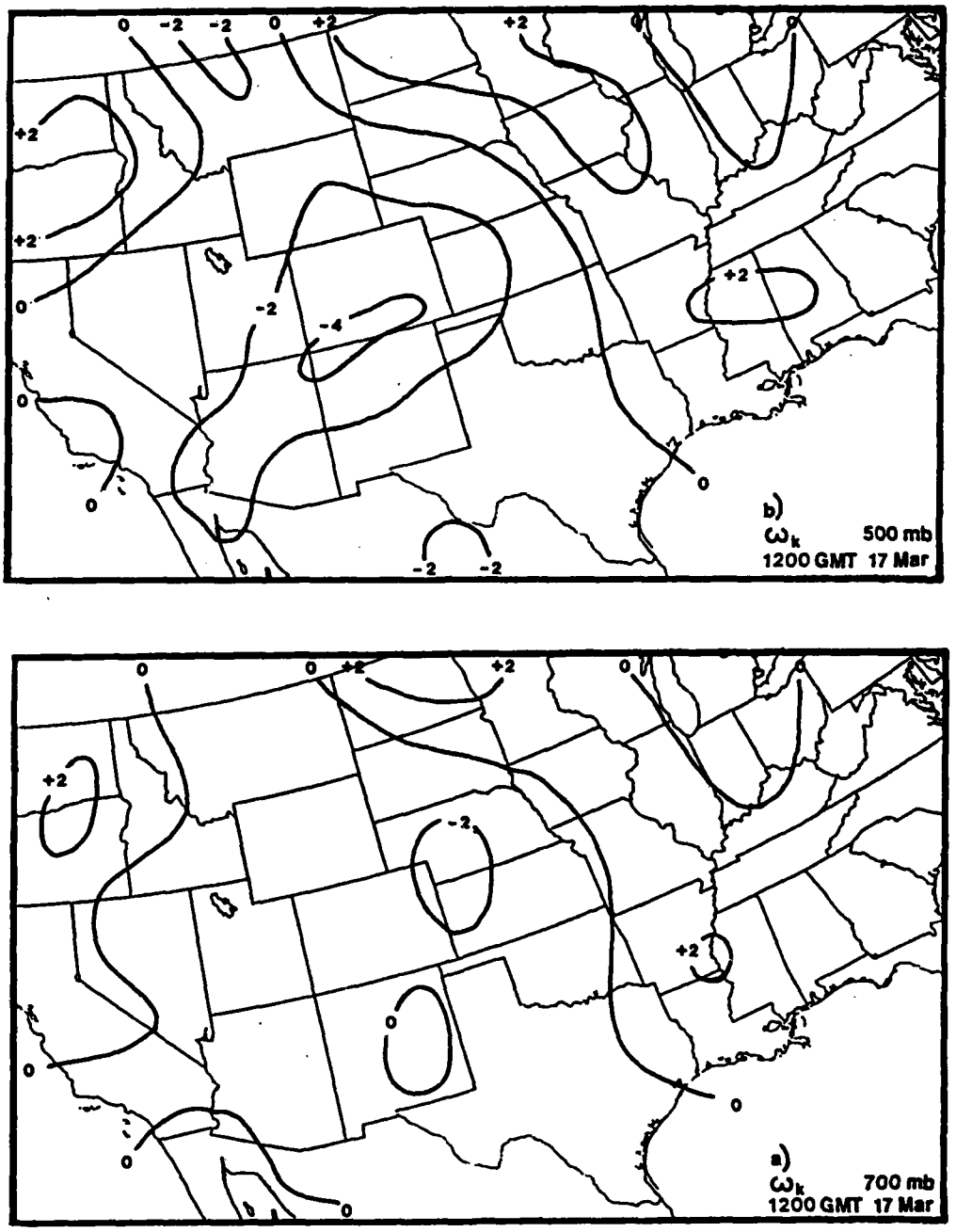

Fig. 6 Kinematic vertical motions (microbars/s) at a) 700 mb and b) 500 mb for 1200 GMT 17 March 1986.

northern New Mexico and southern Colorado, which is north of the 500 mb jet axis. The large values of ω here support the development of the cyclone in southern Colorado. The subsidence along both the east and west coasts is located upwind of the major troughs where negative vorticity advection is occurring.

At 0000 GMT 18 March (Figs. 7a-b), the clouds and precipitation (Fig. 3) again correspond fairly well to the areas of upward kinematic vertical motion. The maximum ascent over central Nebraska coincides with the severe thunderstorms which occurred 6 h earlier. This ω maximum is reflected up to 500 mb, where it is located in the positive vorticity advection related to the trough (Fig. 3). Corresponding to the cyclogenesis, the magnitudes of rising motion have almost doubled at both 700 mb and 500 mb during the past 12 h. One should note that the kinematic method now fails to produce subsidence in the clear region behind the cold front.

Figures 8a-b show kinematic vertical motions at 1200 GMT 18 March. As at the previous times, clouds and precipitation (Fig. 4) coincide well with the upward vertical motion. Thunderstorms are over northeast Nebraska, near the ω maximum, as well as over eastern Texas after 1400 GMT in association with the southernmost maximum of upward motion. Both areas are indicated at the 500 mb level as well. Magnitudes have not changed appreciably at either

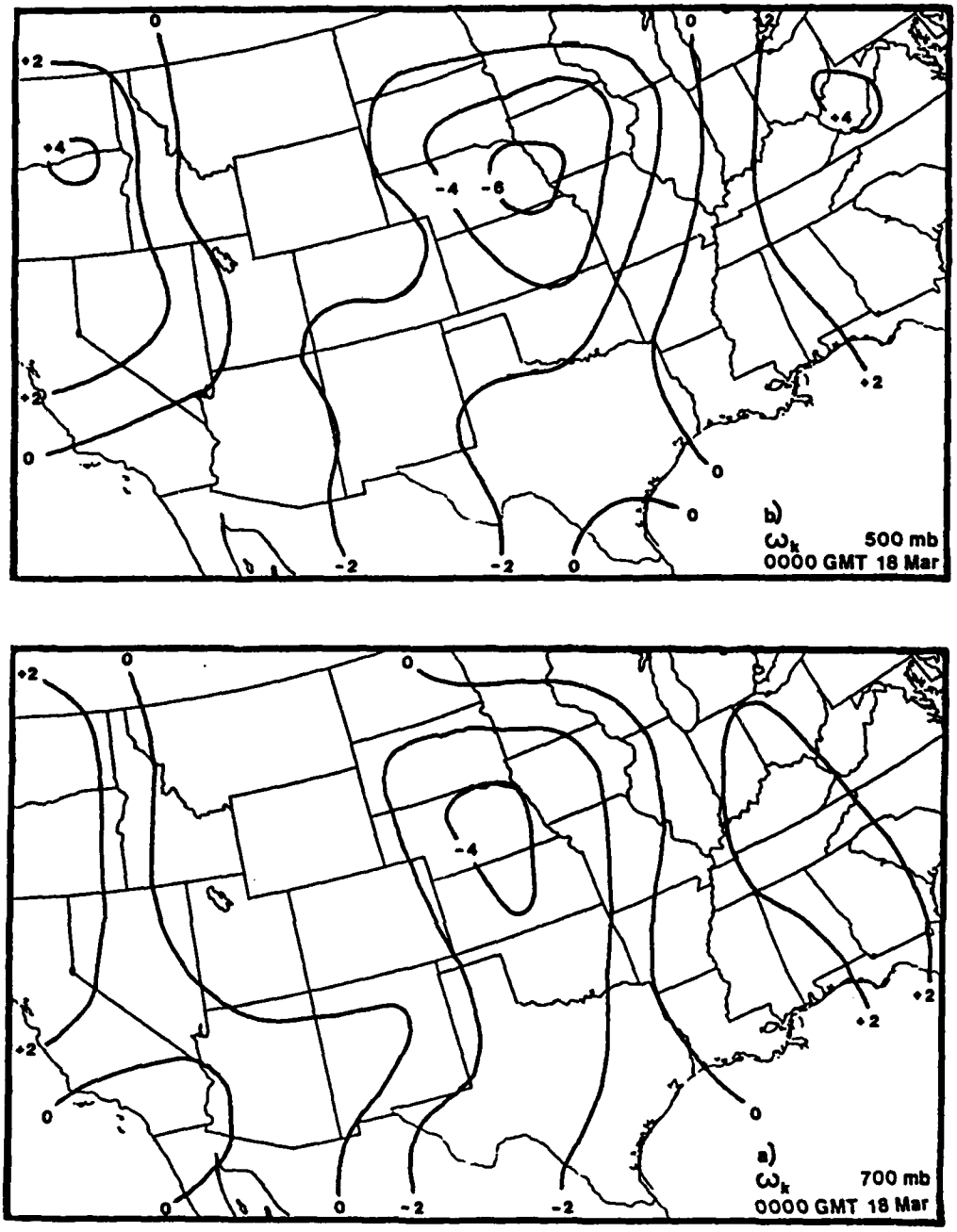

Fig. 7 As in Fig. 6, but for 0000 GMT 18 March 1986.

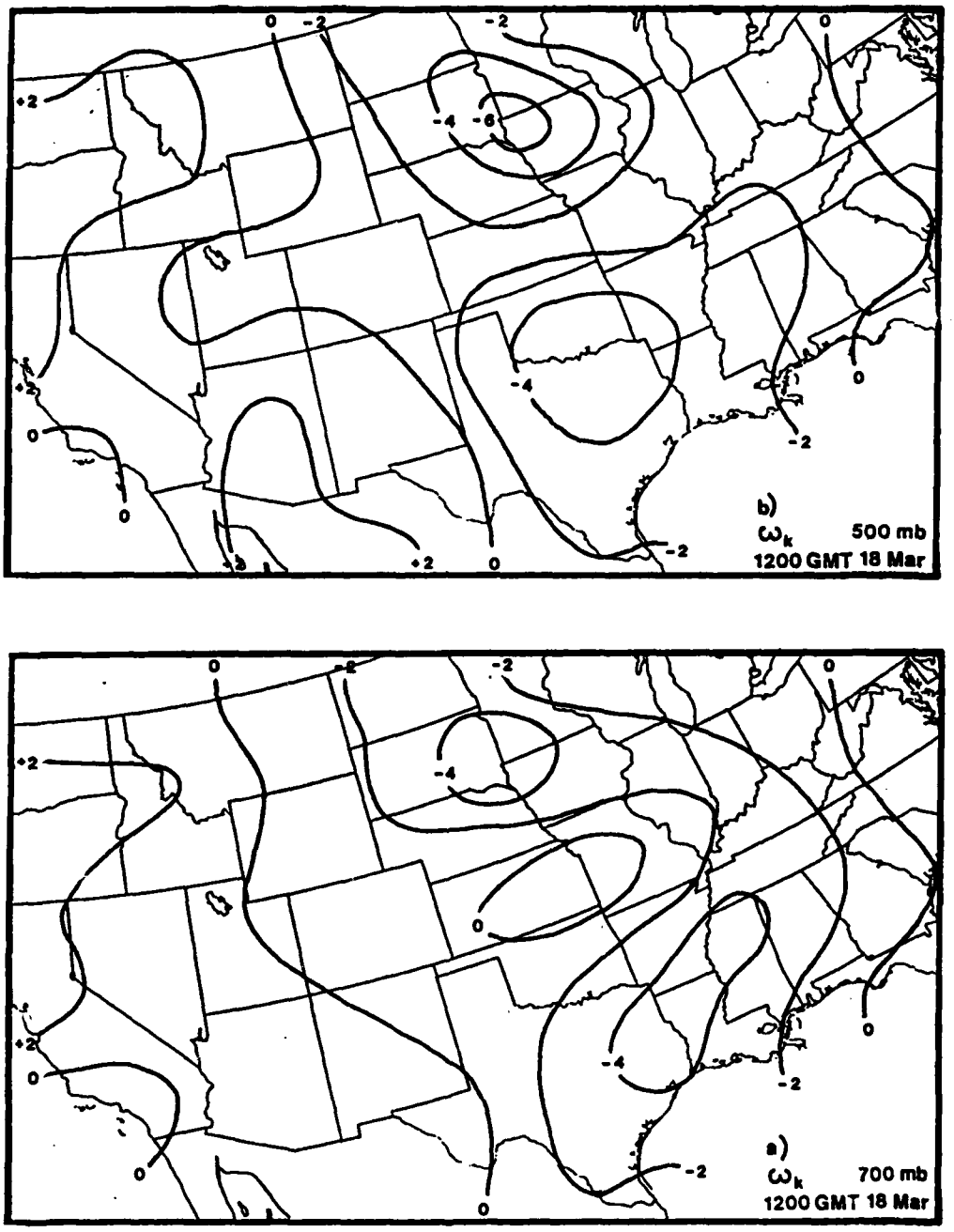

Fig. 8 As in Fig. 6, but for 1200 GMT 18 March 1986.

700 mb or 500 mb, but the centers continue to move to the northeast, ahead of the cyclone. In contrast to the previous time, an area of subsidence at 700 mb over Kansas correlates with the clear slot behind the cold front, although it should extend farther south into Texas.

Finally, by 0000 GMT 19 March (Figs. 9a-b), the two previous centers of maximum upward motion merge and increase to -6.9 and -8.2 microbars/s at 700 mb and 500 mb, respectively. They continue to move ahead of the surface low and 500 mb trough (Fig. 5). For the most part, clouds and precipitation occur in regions of rising motion. For example, a severe thunderstorm occurred at this time over southeast Missouri in association with the strong rising motion through 500 mb. In fact, strong thunderstorms developing ahead of the entire cold front agree with ω pattern of ascent. On the other hand, some snowfall in western Nebraska, Wyoming and Colorado is outside the region of upward motion. In addition, the area of subsidence does not adequately reflect the clear wedge between the cold front and the trailing surface trough. The ω fields do have subsidence west of the Rockies where negative vorticity advection is occurring in the rear of the 500 mb trough.

Kinematic vertical motions are derived from the calculation of divergence as described earlier. Figures 10a-d show divergence fields at 700 mb for the four times. In

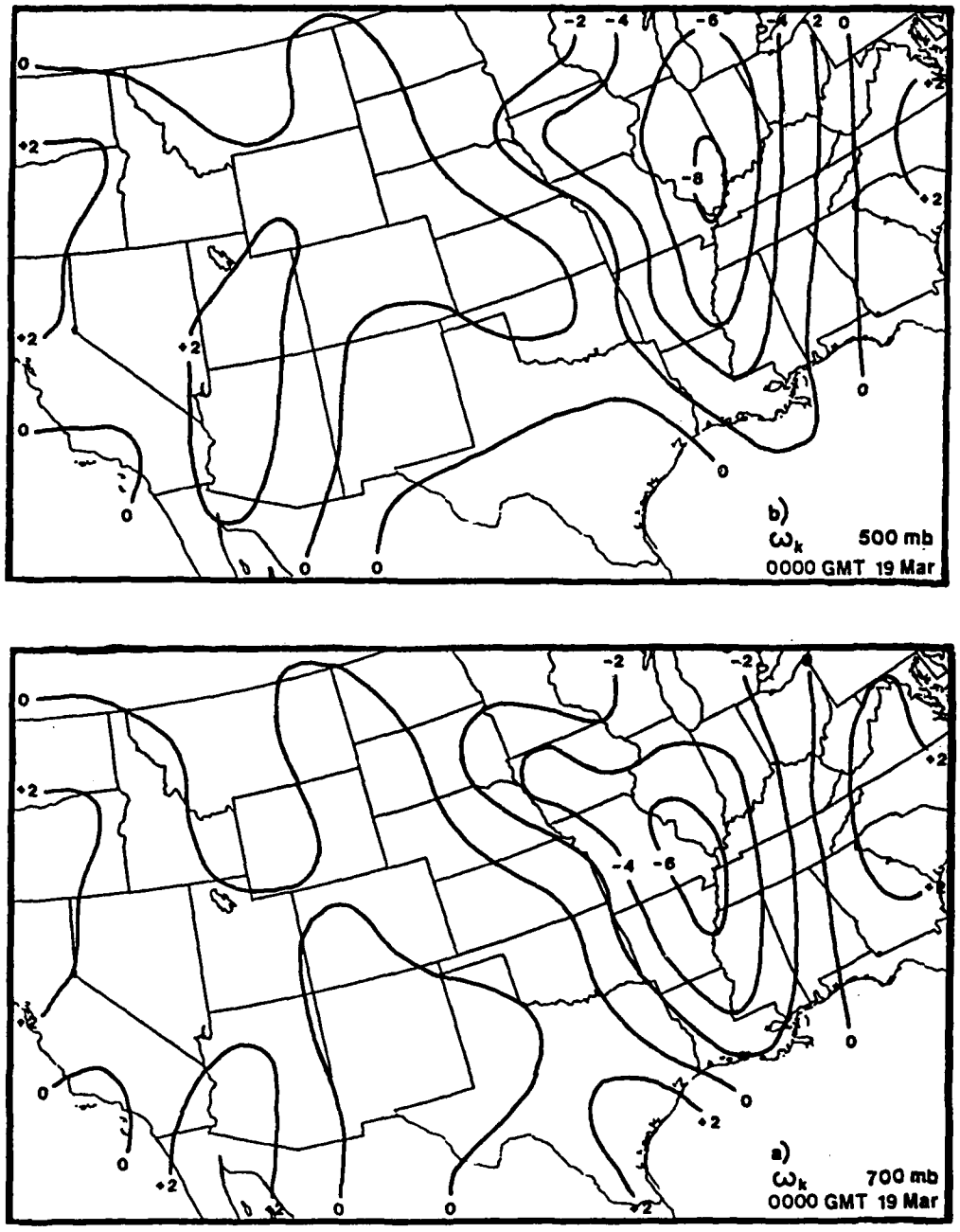

Fig. 9 As in Fig. 6, but for 0000 GMT 19 March 1986.

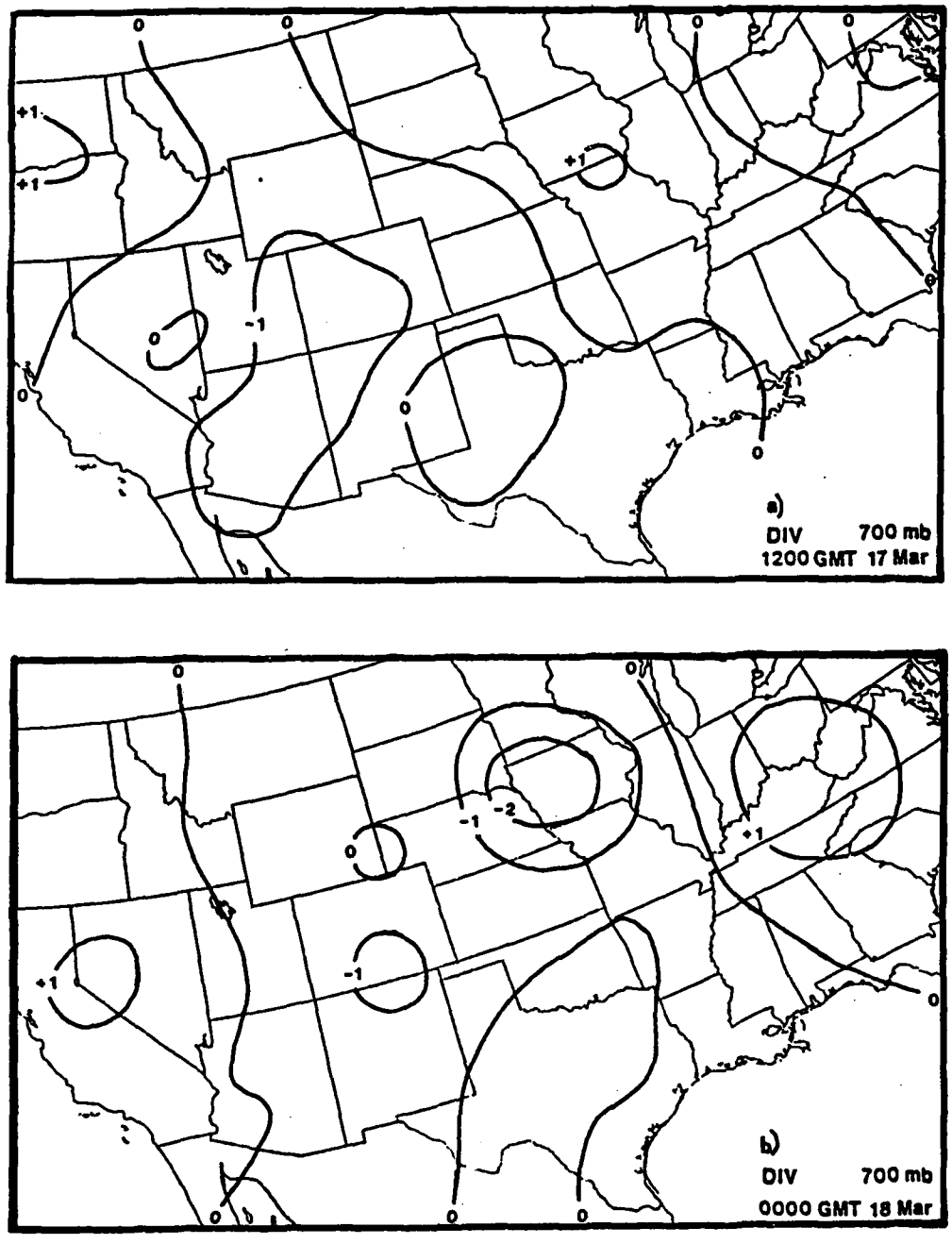

Fig. 10 Horizontal velocity divergence (10^{-5} s^{-1}) at 700 mb for a) 1200 GMT 17 March 1986, b) 0000 GMT 18 March 1986, c) 1200 GMT 18 March 1986, and d) 0000 GMT 19 March 1986.

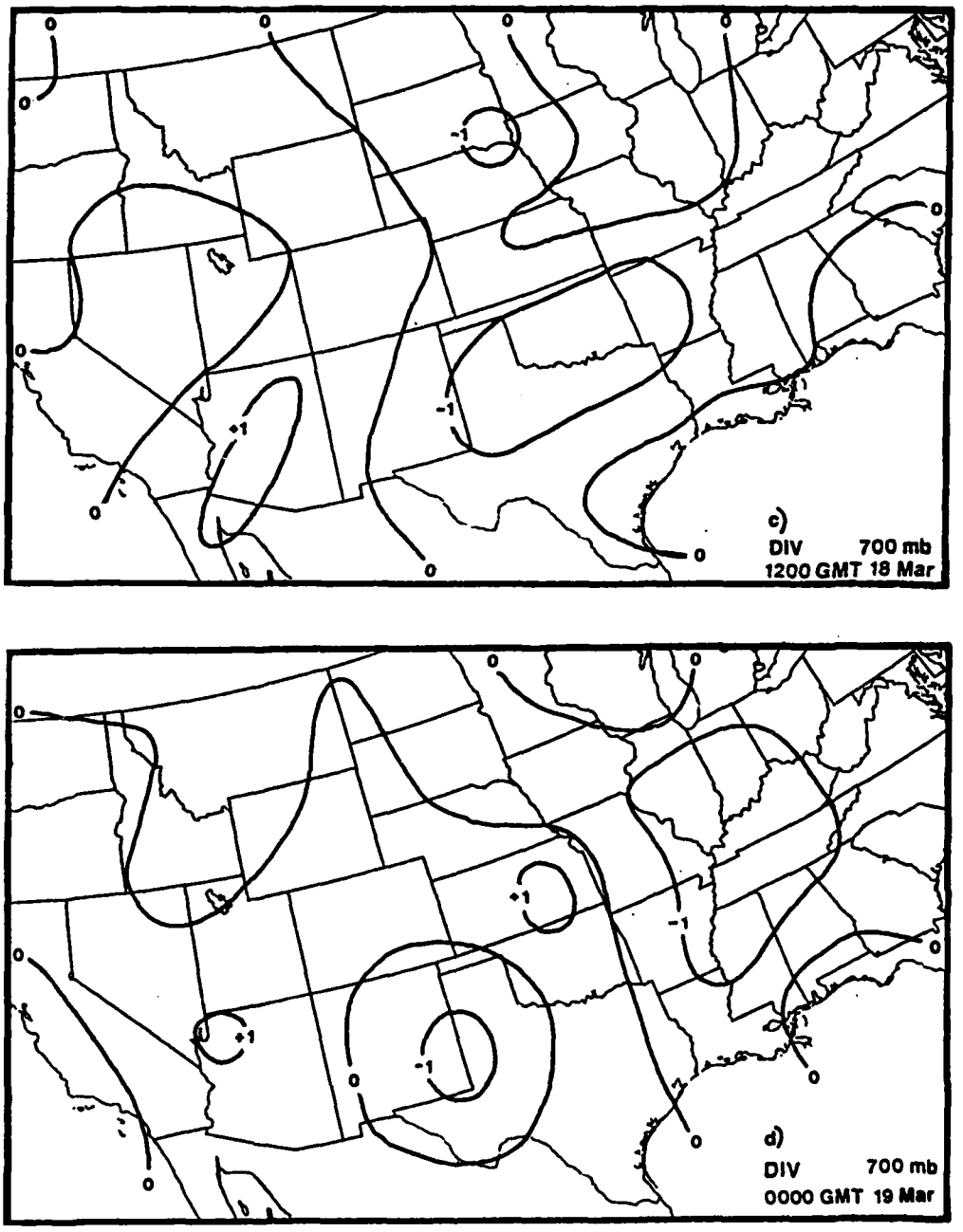

Fig. 10 (continued).

general, one should note that areas of convergence align fairly well with the centers of upward motion (Figs. 6-9), but the divergence values are fairly weak. The strongest convergence of -2.7×10^{-5} s^{-1} is at 0000 GMT 18 March (Fig. 10b) over western Iowa, corresponding to the severe thunderstorm that occurred in eastern Nebraska 6 h earlier. Although one cannot quantify vertical motion based on divergence at any one level, the results for this case of major cyclogenesis suggest that qualitative ω patterns can be obtained from a single level of divergence. Of course, such an inference is frequently made by operational meteorologists.

The next three sections of results were all derived from the same basic quasi-geostrophic concepts; therefore, ω patterns are expected to be rather similar. As noted earlier however, there will be some differences because of the slightly differing assumptions and methods of calculating the particular forcing functions. The traditional omega equation method is the first of these routines to be analyzed. Figures 11a-b show 700 and 500 mb vertical motions at 1200 GMT 17 March. The broad area of upward vertical motion is correctly situated ahead of the surface cold front and the upper level trough (Fig. 2). In addition, a center of subsidence at 700 mb is located over New Mexico, just behind the cold front.

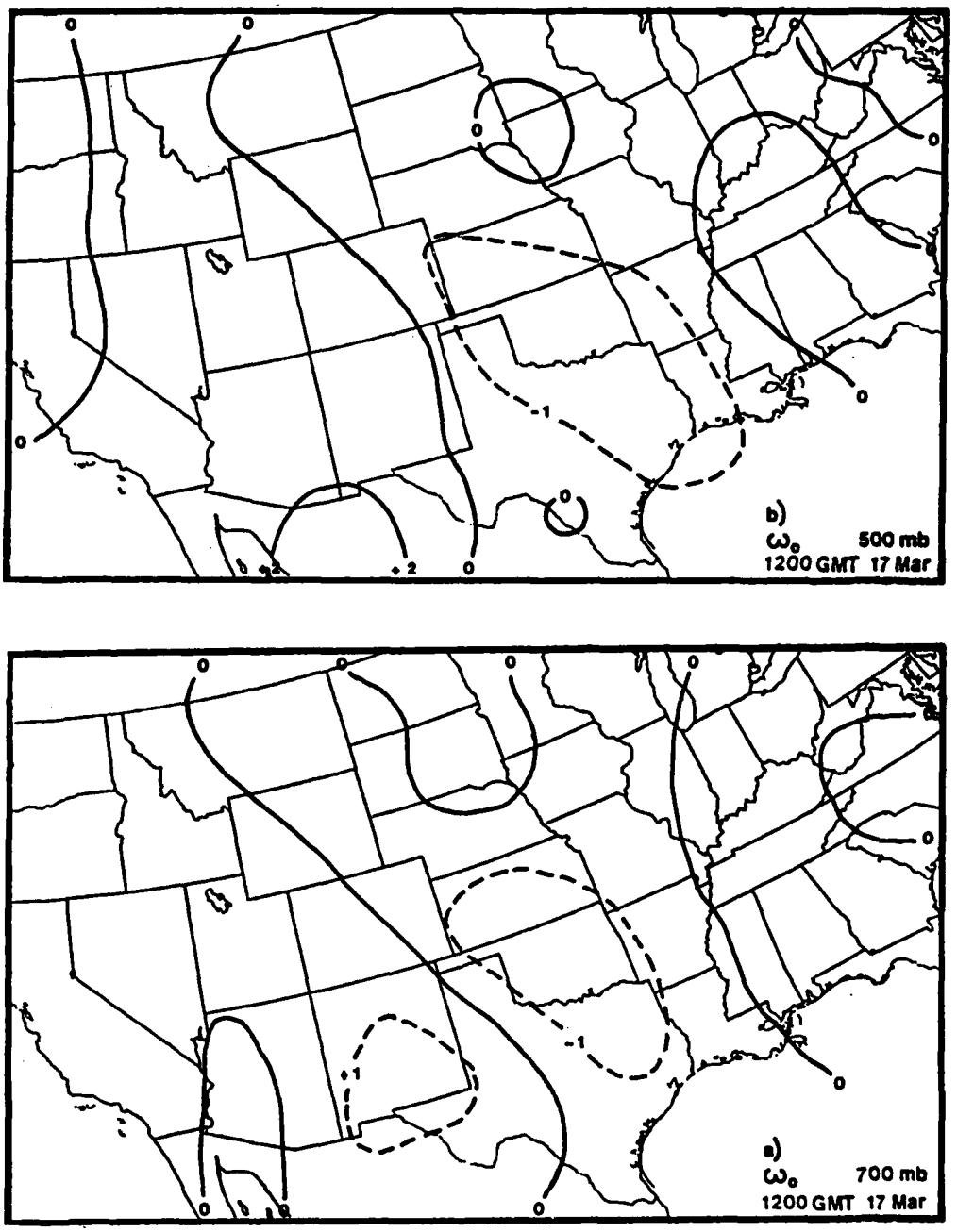

Fig. 11 Vertical motions (microbars/s) from the traditional omega equation at a) 700 mb and b) 500 mb for 1200 GMT 17 March 1986.

Notice that magnitudes are much weaker than those from the kinematic procedure (Fig. 6); maximum values are only -1.7 and -1.9 microbars/s at 700 and 500 mb, respectively. A major difference with the kinematic motions is that the omega equation procedure yields subsidence where snow was falling over western Montana, Idaho, northern Utah, and Colorado. In addition, the omega equation method, like its kinematic counterpart, does not produce rising motion near the thunderstorm over San Diego, CA.

At 0000 GMT 18 March (Figs. 12a-b), the omega equation vertical motion patterns at 700 and 500 mb are similar. In each case, a center of ascent is located over the middle Mississippi River Valley ahead of the surface low (Fig. 3), while there is an area of subsidence over west Texas and New Mexico that is in a clear region west of the cold front. The zero line through central Texas aligns with the location of the cold front. Magnitudes are considerably stronger than at the previous time, but the location of the upward motion maximum does not properly correspond to the precipitation field. Specifically, no precipitation fell in southeastern Missouri where the -4.0 microbar/s maximum is situated. Conversely, the severe weather over central Nebraska occurred where the traditional omega scheme produced subsidence at 700 mb. While the precipitation over Montana is in a region of upward motion, it does not extend far enough

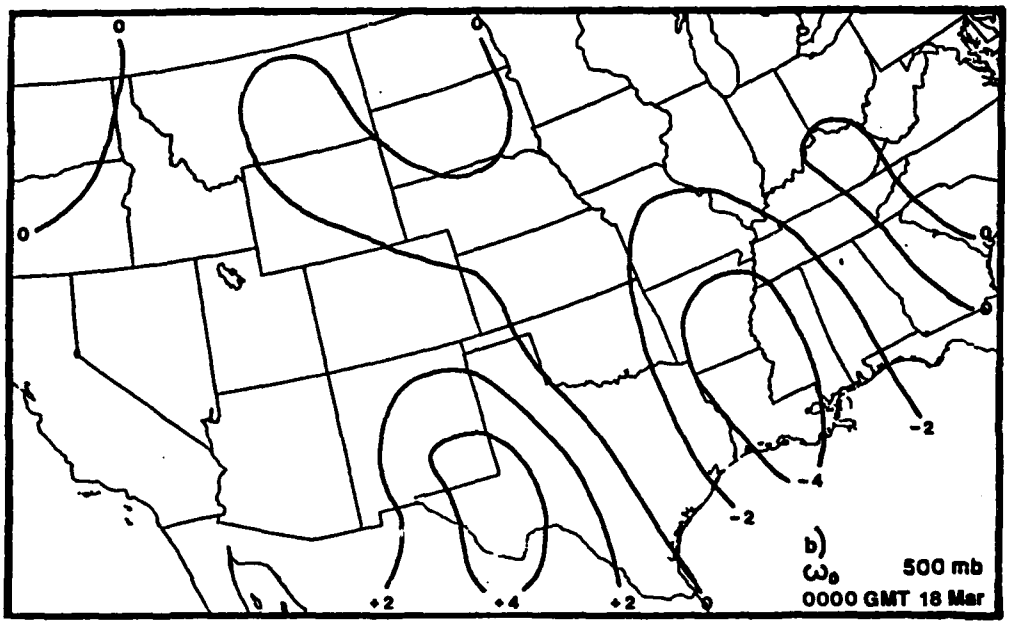

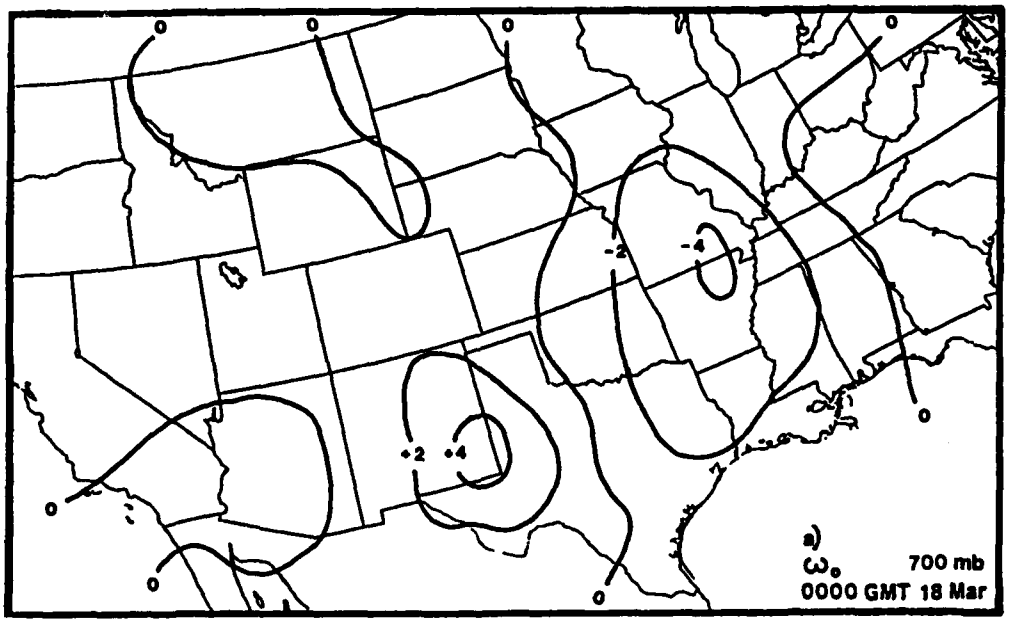

Fig. 12 As in Fig. 11, but for 0000 GMT 18 March 1986.

south to include the rain in Wyoming, Utah, and Colorado.

At 1200 GMT 18 March (Figs. 13a-b), there again is widespread upward motion ahead of the surface cyclone and 500 mb trough (Fig. 4), and there is subsidence behind the cold front. The magnitudes now are weaker at both levels, despite the presence of thunderstorms. The maximum upward motion at 700 mb now corresponds better to the showers and thunderstorms in Arkansas, Missouri and Illinois; however, the thunderstorms in Nebraska along with the snow over the Dakotas, Montana, Wyoming, and Colorado are located in a region of subsidence. Maximum subsidence over western Texas aligns well with the clear region behind the cold front, but should extend farther north into Kansas.

Areas of rising motion at 0000 GMT 19 March (Fig. 14a-b) again are located ahead of the surface low and 500 mb trough (Fig. 5), and there is sinking motion in the clear slot behind the cold front. The magnitudes have doubled over the past 12 h; however, the strongest upward motion at 700 mb does not align with the thunderstorms which occurred from Missouri through Mississippi along the cold front. In addition, the snow over Minnesota, the Dakotas, and Nebraska is located in a region of subsidence. Conversely, rising motion over much of the Rockies corresponds nicely with showers there.

In general it appears that the omega equation vertical motions do not agree with the clouds/weather as did

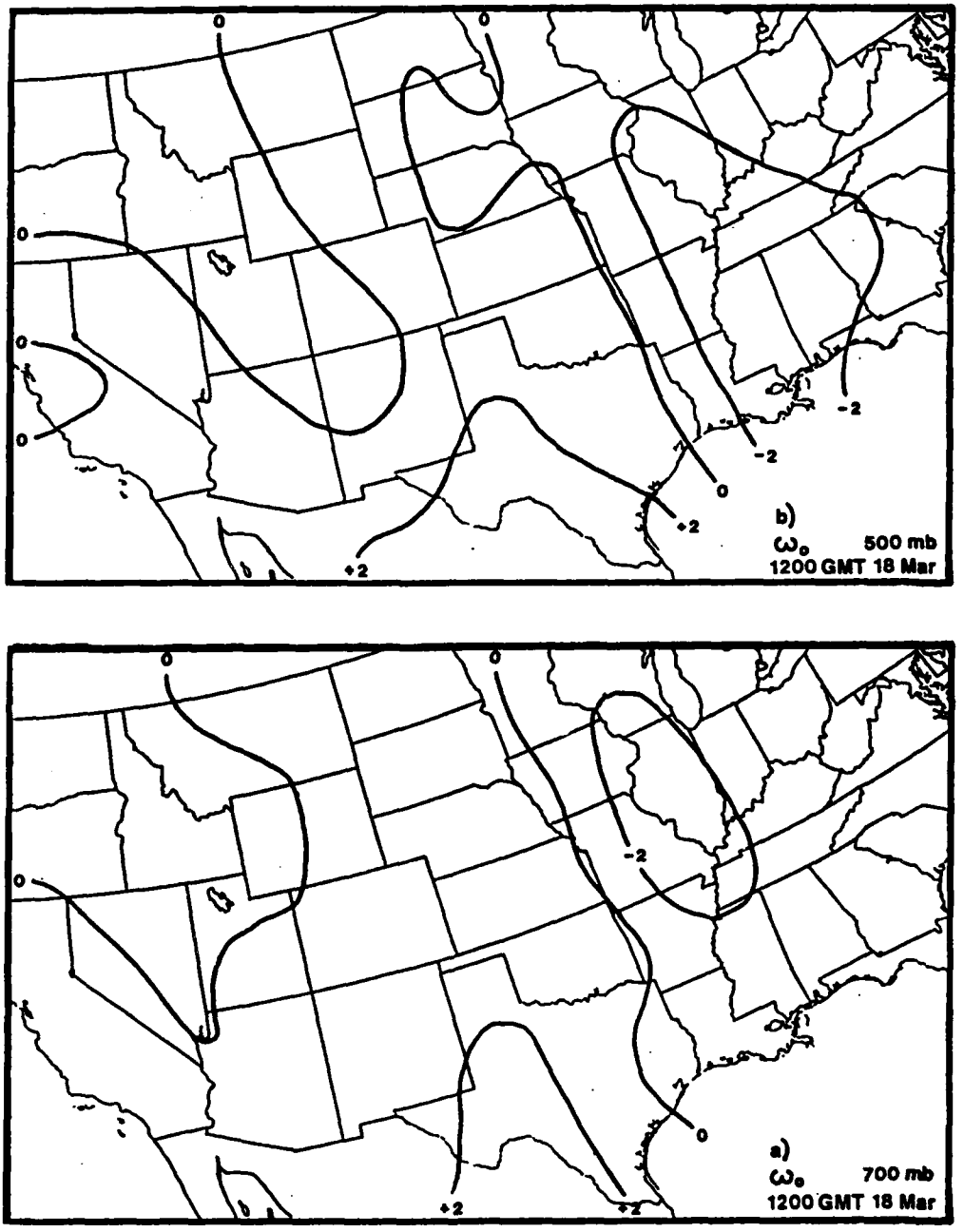

Fig. 13 As in Fig. 11, but for 1200 GMT 18 March 1986.

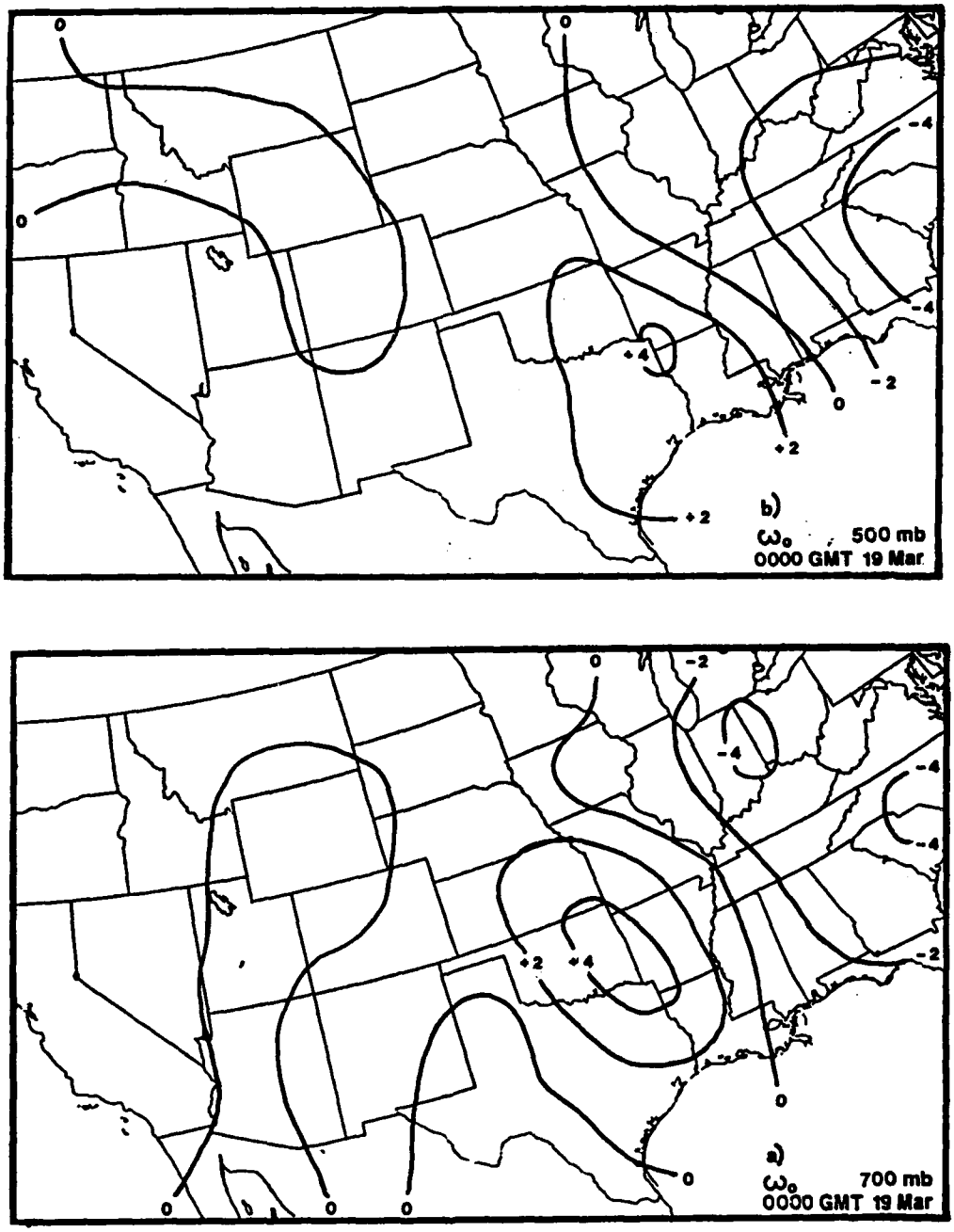

Fig. 14 As in Fig. 11, but for 0000 GMT 19 March 1986.

the kinematic motions. The scoring procedure in the next section will objectively evaluate this hypothesis.

As described earlier, a problem of the traditional omega equation is that the two forcing terms in (5) can cancel each other. Furthermore, Durran and Snellman (1987) concluded that the individual terms have no physical significance on their own because changes in mean wind cause changes in the advection of thermal vorticity. Therefore, two identical weather systems moving at different speeds would produce different forcing terms despite the fact that the same vertical motion field would result. Thus, the sum of the two terms must be considered to get ω. With these points in mind, Fig. 15a shows the contribution of differential vorticity advection at 700 mb on 1200 GMT 17 March, while Fig. 15b illustrates the contribution from the horizontal Laplacian of thickness advection at the same time and level. By comparing the two fields, one can see that both terms contribute to the rising motion ahead of the surface front (Fig. 2); however, some opposing signs can be seen over the Dakotas, eastern Kansas, and most of the west coast. The fields are relatively weak, so neither term is overly dominant.

The situation is similar at 0000 GMT 18 March (Fig. 16a-b). Both terms produce rising motion ahead of the surface cyclone (Fig. 3); however, there also are areas of opposing signs. For example, the thickness term yields

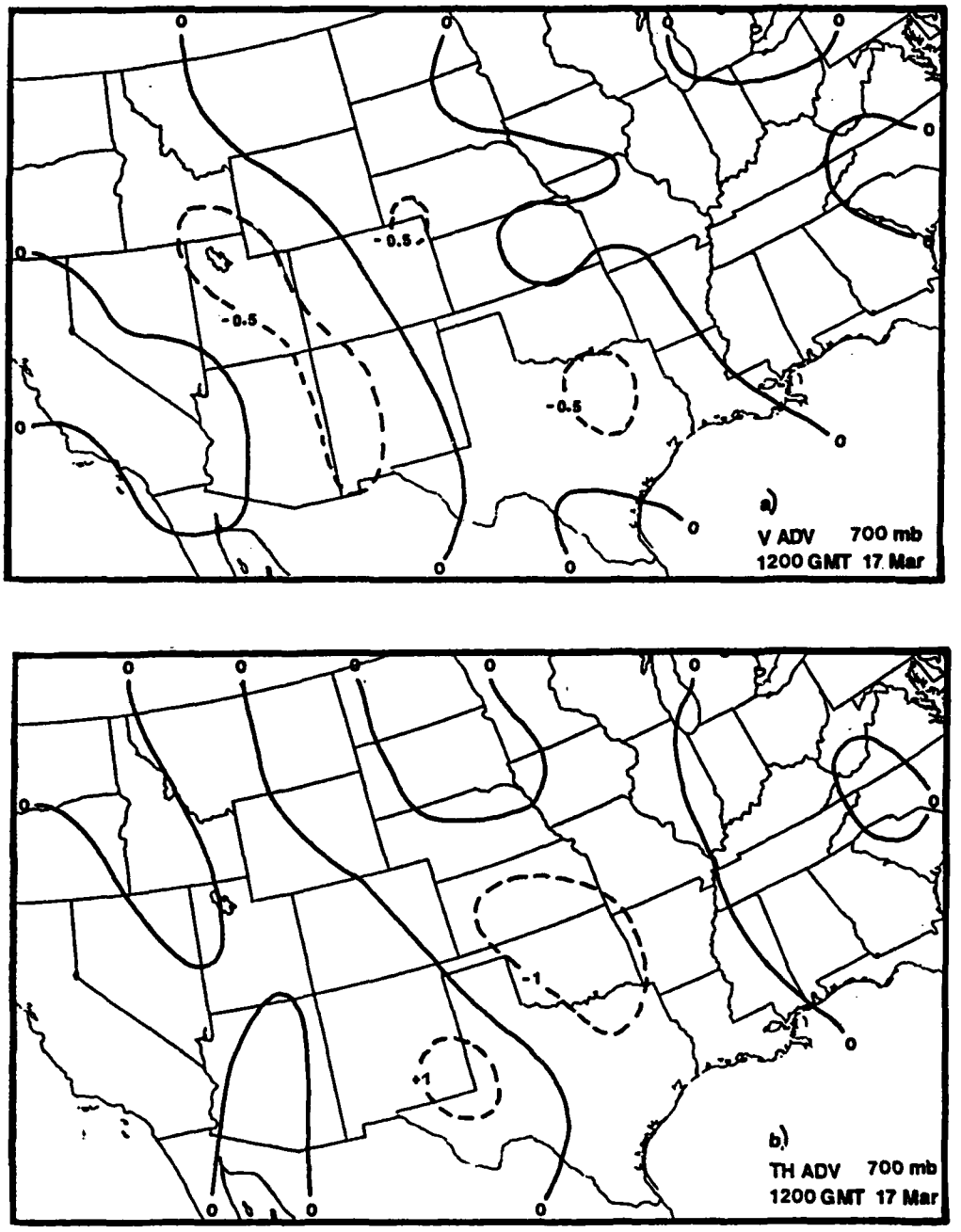

Fig. 15 Components of traditional omega equation vertical motion (microbars/s) at 700 mb on 1200 GMT 17 March 1986 due to a) differential vorticity advection and b) the horizontal Laplacian of thickness advection.

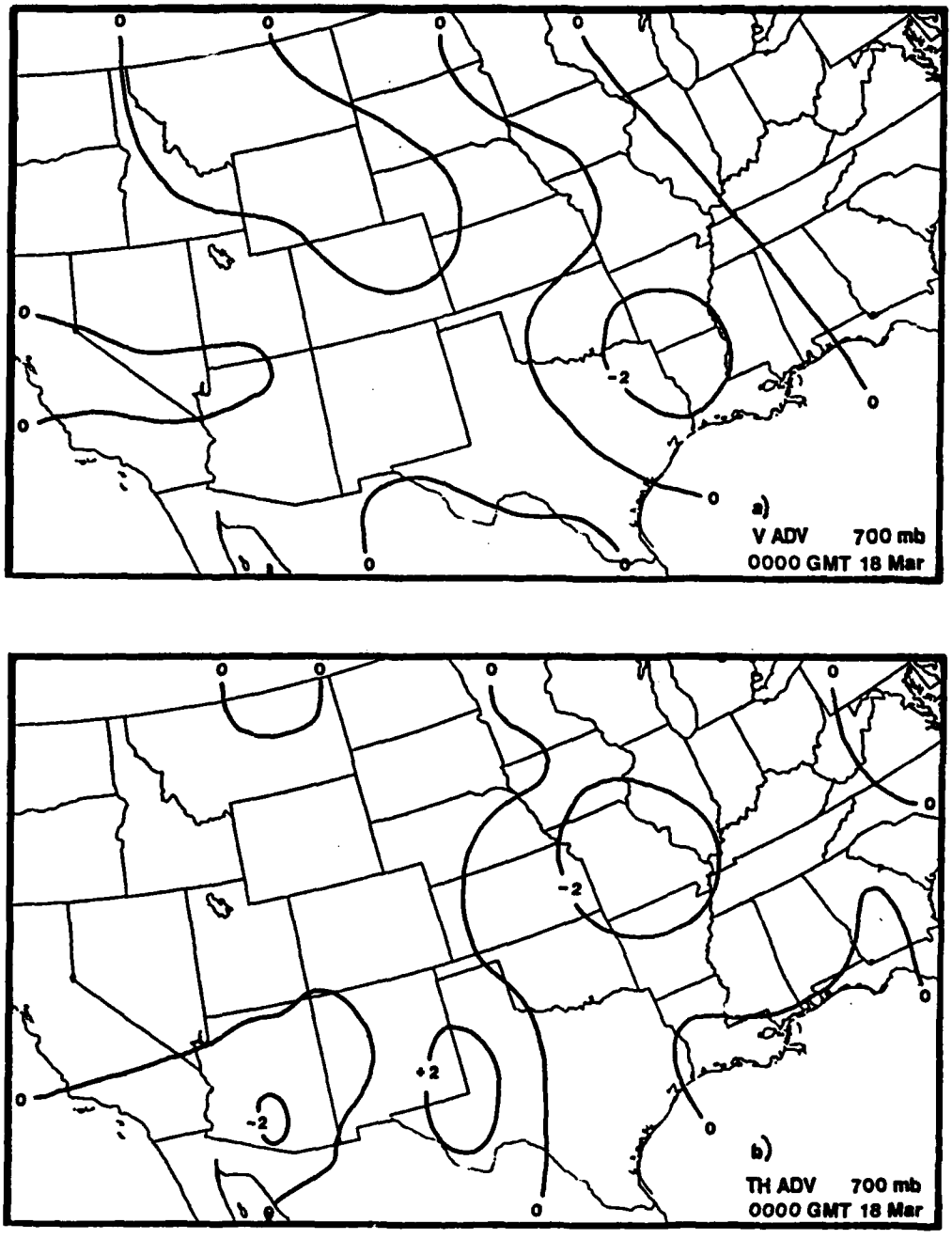

Fig. 16 As in Fig. 15, but for 0000 GMT 18 March 1986.

upward motion over southeastern Nebraska where the hail-storm occurred 6 h earlier, while the vorticity term produces subsidence in that region. The two terms nearly cancel each other in producing the resultant ω field (Fig. 12a). However, over Montana, Wyoming, Colorado and western Nebraska, the thickness term produces subsidence while the advection term shows ascent. The vorticity term dominates over most of the area, to give resulting upward motion. On the other hand, the thickness term dominates over southern California and Arizona, resulting in net upward motion in that region.

At 1200 GMT 18 March (Fig. 17a-b), the vorticity and thickness terms both produce rising motion ahead of the cyclone (Fig. 4). Once again, however, the vorticity advection term yields upward motion which corresponds better to the snow over Montana, Wyoming and Colorado. As at the first time, the fields are too weak for either term to dominate.

Finally, both the vorticity advection and the thick-ness advection terms at 0000 GMT 19 March (Figs. 18a-b) indicate rising motion ahead of the front (Fig. 5), but the component from the vorticity term correlates better with the precipitation areas over the Rockies. In addition, magnitudes of the thickness contribution are much greater than those from the vorticity term although their signs are similar.

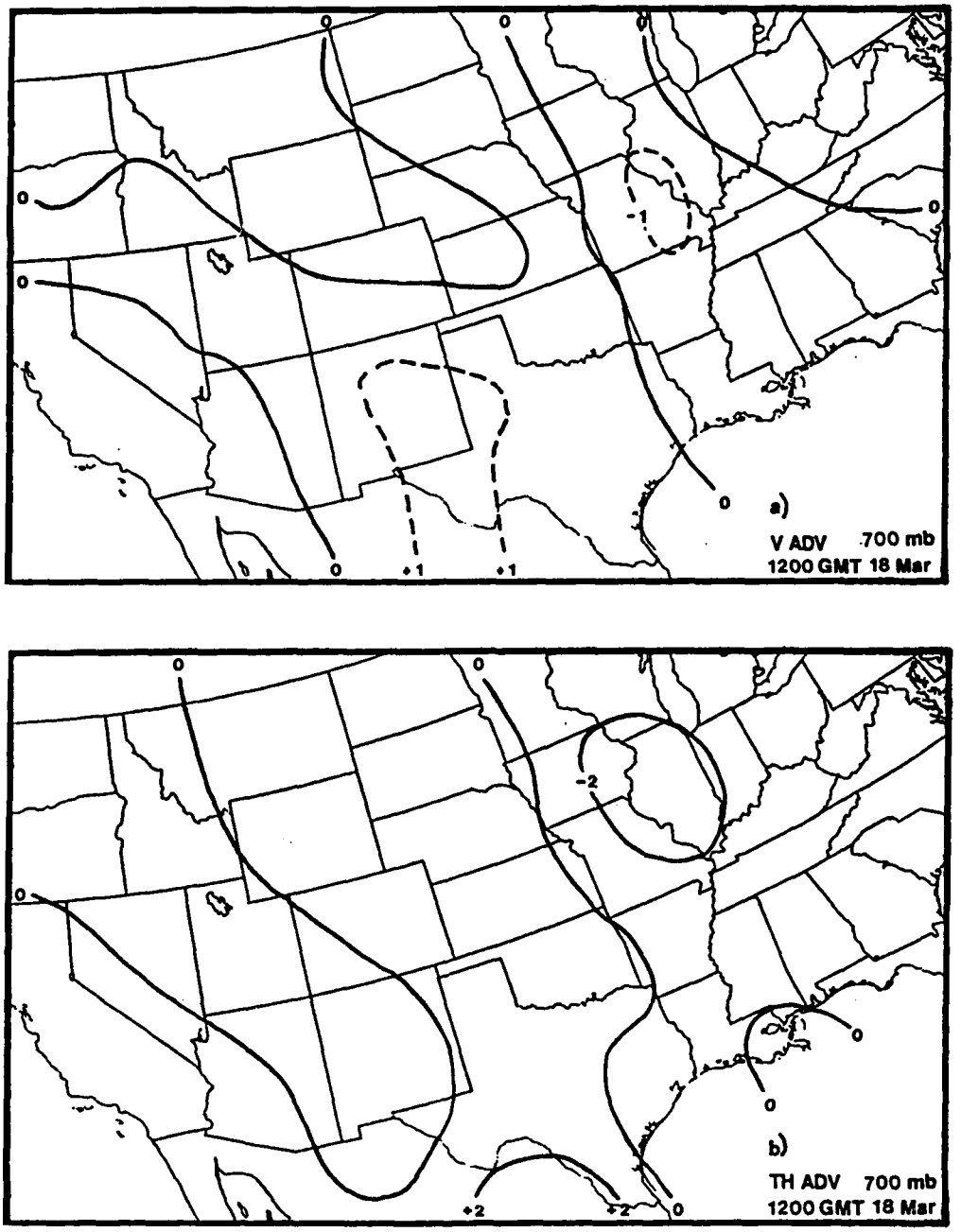

Fig. 17 As in Fig. 15, but for 1200 GMT 18 March 1986.

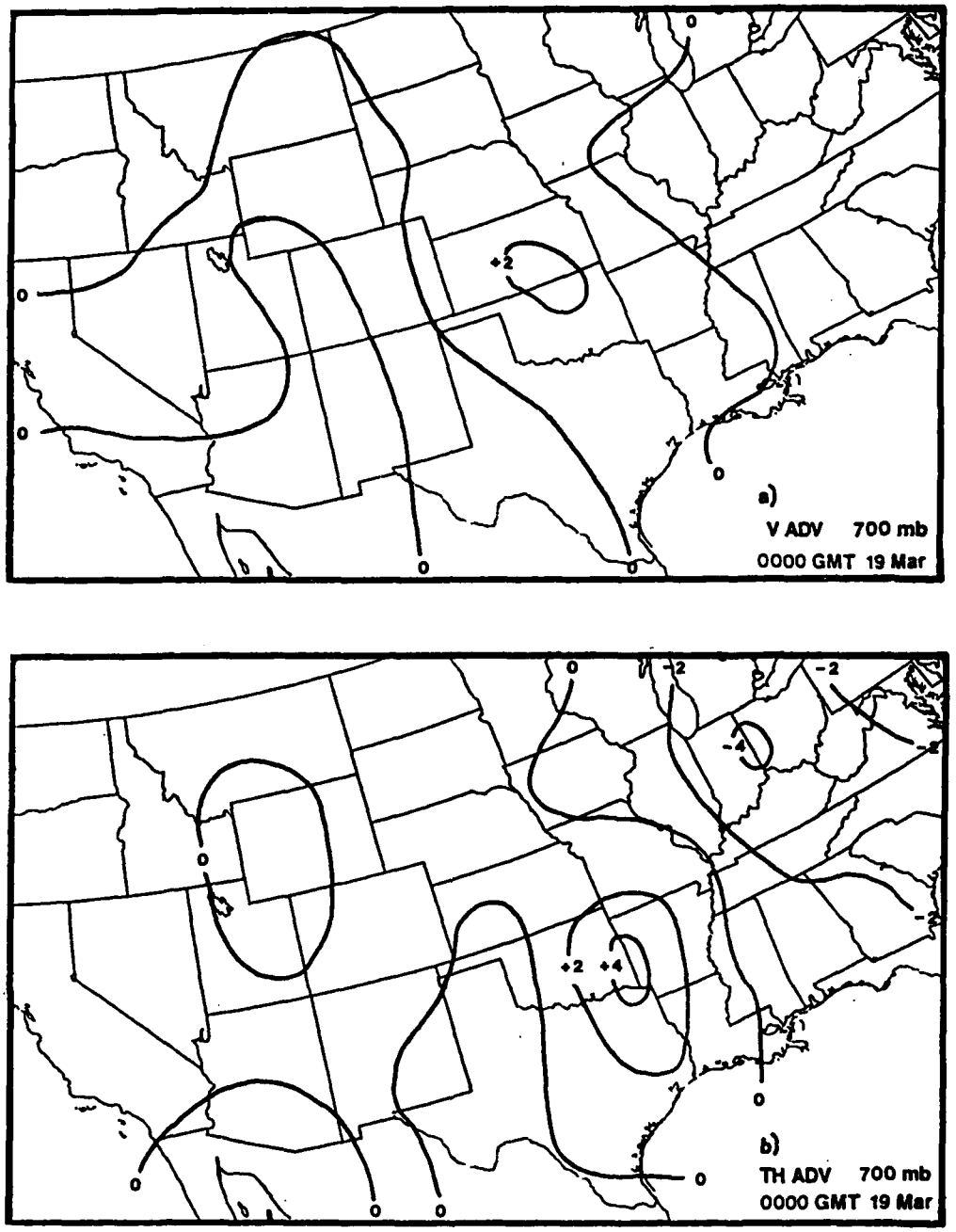

Fig. 18 As in Fig. 15, but for 0000 GMT 19 March 1986.

The problem of term cancellation described above was avoided by Trenberth (1978), who developed a method of calculating vertical motion from a single forcing function when assuming a negligibly small deformation term. Durran and Snellman (1987) noted the following: "If a forecaster must estimate the [quasi-geostrophic] vertical velocity without the aid of special computer programs, he will probably get the best result (and certainly get it with least effort) by using the Trenberth-Sutcliffe approximation". In the current case, differences in ω fields from the traditional and Trenberth formulations are subtle at all times and levels. Where differences are apparent, however, they will be noted in the subsequent discussion. Only analyses with deformation included are presented since, as noted earlier, there was very little difference with versions neglecting that process.

The resultant ω field at 700 mb for 1200 GMT 17 March (Fig. 19a) shows great similarity with the one calculated by the traditional method (Fig. 11a). The only difference is at 500 mb (Fig. 19b) where an area of weak ascent over Arizona did not show up in the traditional method (Fig. 11b). This region corresponds to an area of showers (Fig. 2).

At 0000 GMT 18 March (Fig. 20a), the ω field is once again very similar to that from the traditional formulation (Fig. 12a). Strong rising motion is ahead of the

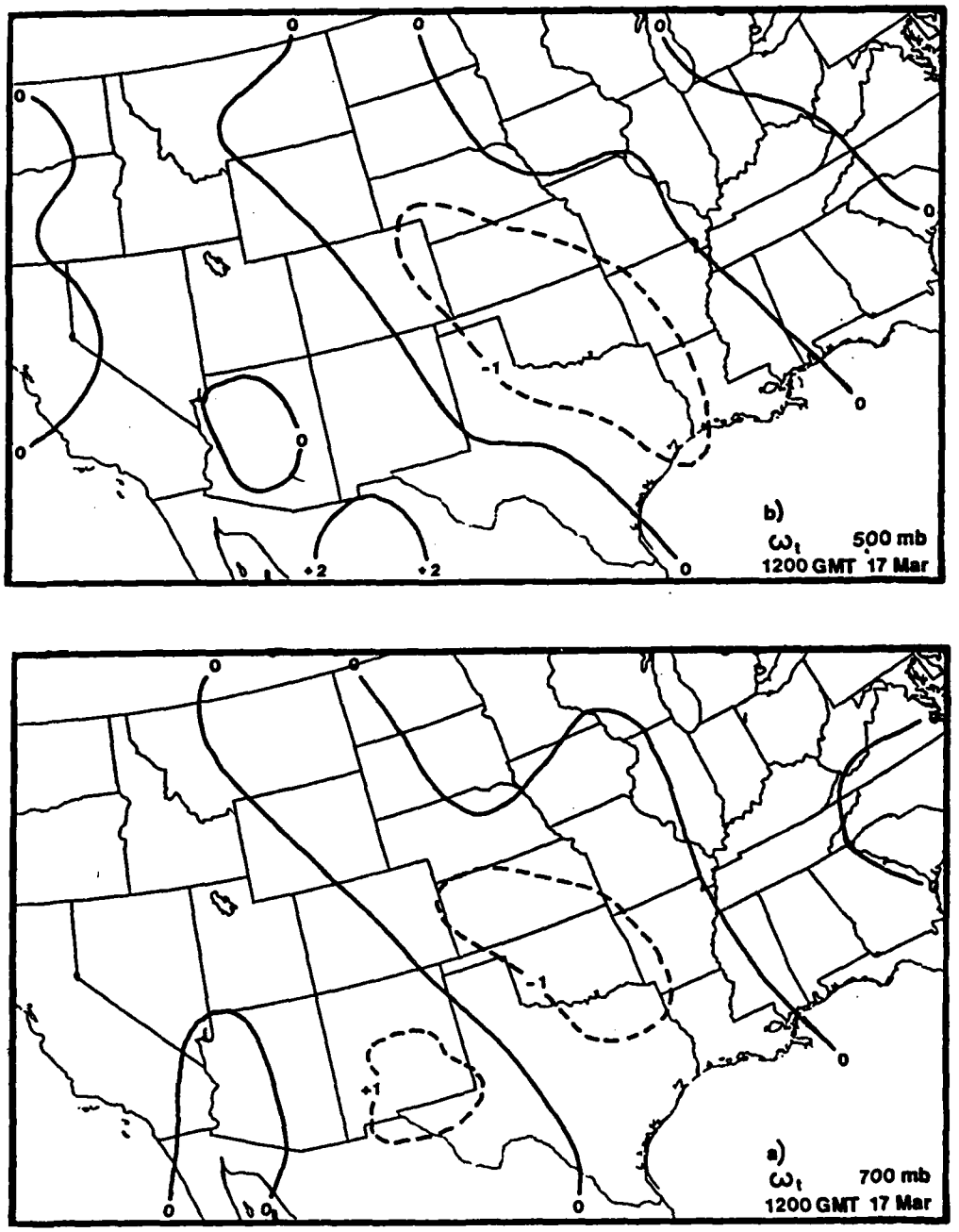

Fig. 19 Vertical motions (microbars/s) from Trenberth's form of the omega equation at a) 700 mb and b) 500 mb for 1200 GMT 17 March 1986.

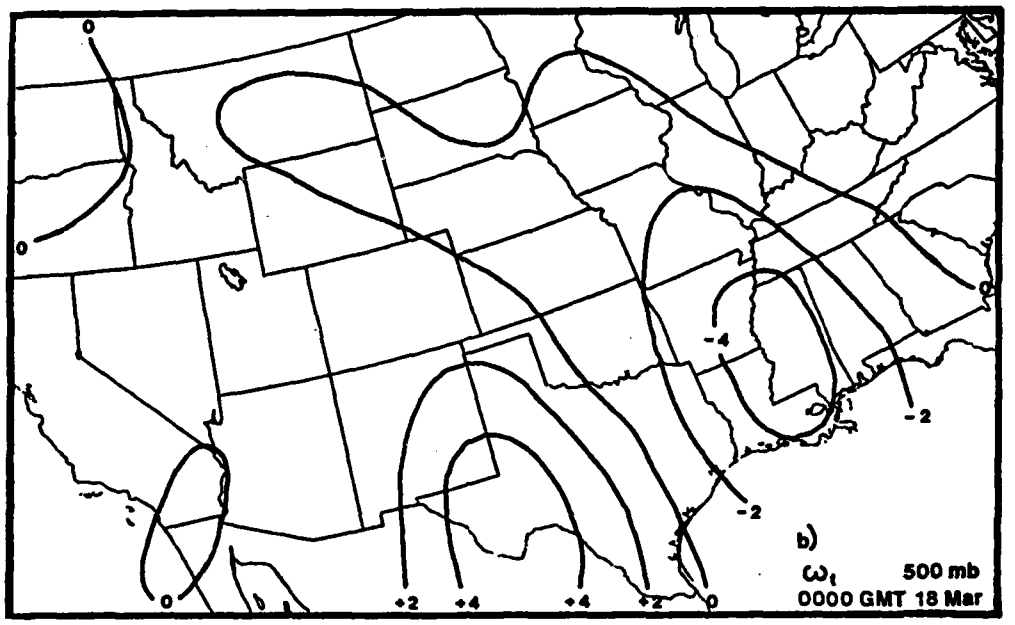

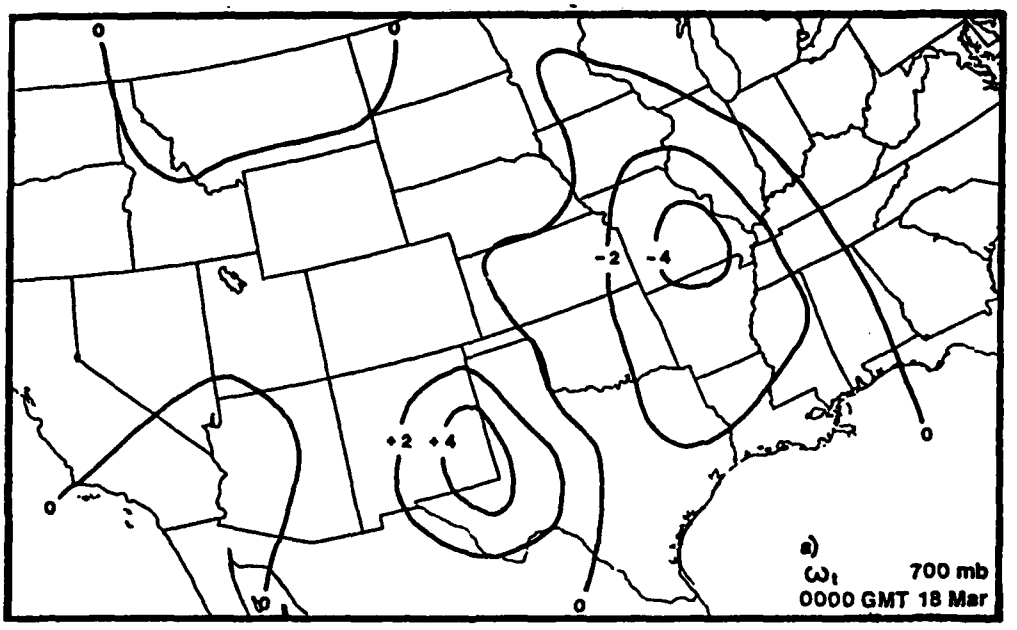

Fig. 20 As in Fig. 19, but for 0000 GMT 18 March 1986.

cyclone (Fig. 3), with comparable subsidence behind the cold front. A difference at 700 mb is that Trenberth's method does not extend the rising motion as far south into Colorado; therefore, it does not align with the precipitation pattern as well as results from the traditional approach. At 500 mb (Fig. 20b) the region of upward motion is again over southern California, but it was not produced by the traditional technique (Fig. 12b). As at the previous time, this area experienced showers.

Figures 21a-b depict the vertical motion fields at 1200 GMT 18 March. Patterns at 700 and 500 mb again resemble those produced by the traditional omega equation (Figs. 13a-b). Moderate rising motion is computed ahead of the cold front (Fig. 4), with subsidence in the clear area behind the front over west Texas. The differences are again over southern California where Trenberth's procedure yields rising motion while the traditional scheme produces subsidence. Since clouds in this area are scattered, results from the traditional method apparently are more appropriate.

At 0000 GMT 19 March (Fig. 22a), the Trenberth ω field at 700 mb again shows rising motion ahead of the cold front (Fig. 5), and subsidence behind it in the clear slot, similar to that from the traditional routine (Fig. 14a). However, magnitudes of ascent over the Ohio River Valley are much weaker from Trenberth's approach, which is

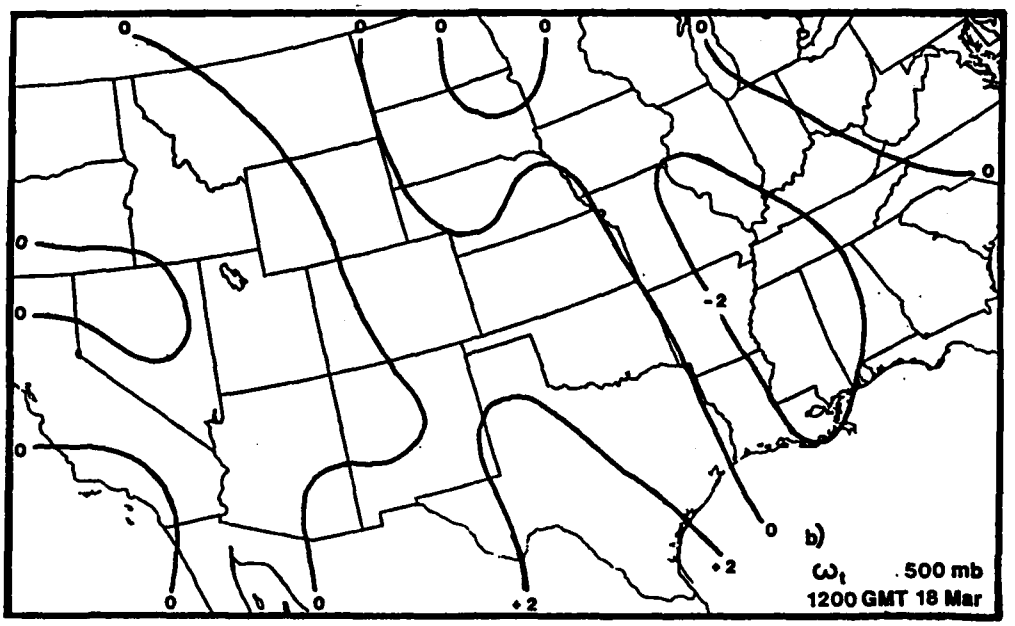

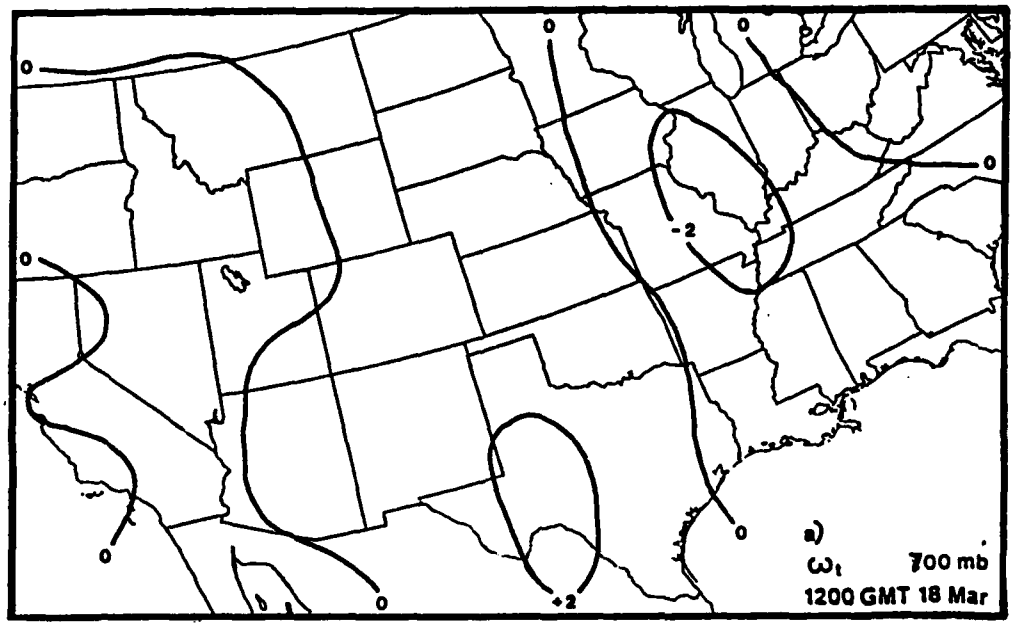

Fig. 21 As in Fig. 19, but for 1200 GMT 18 March 1986.

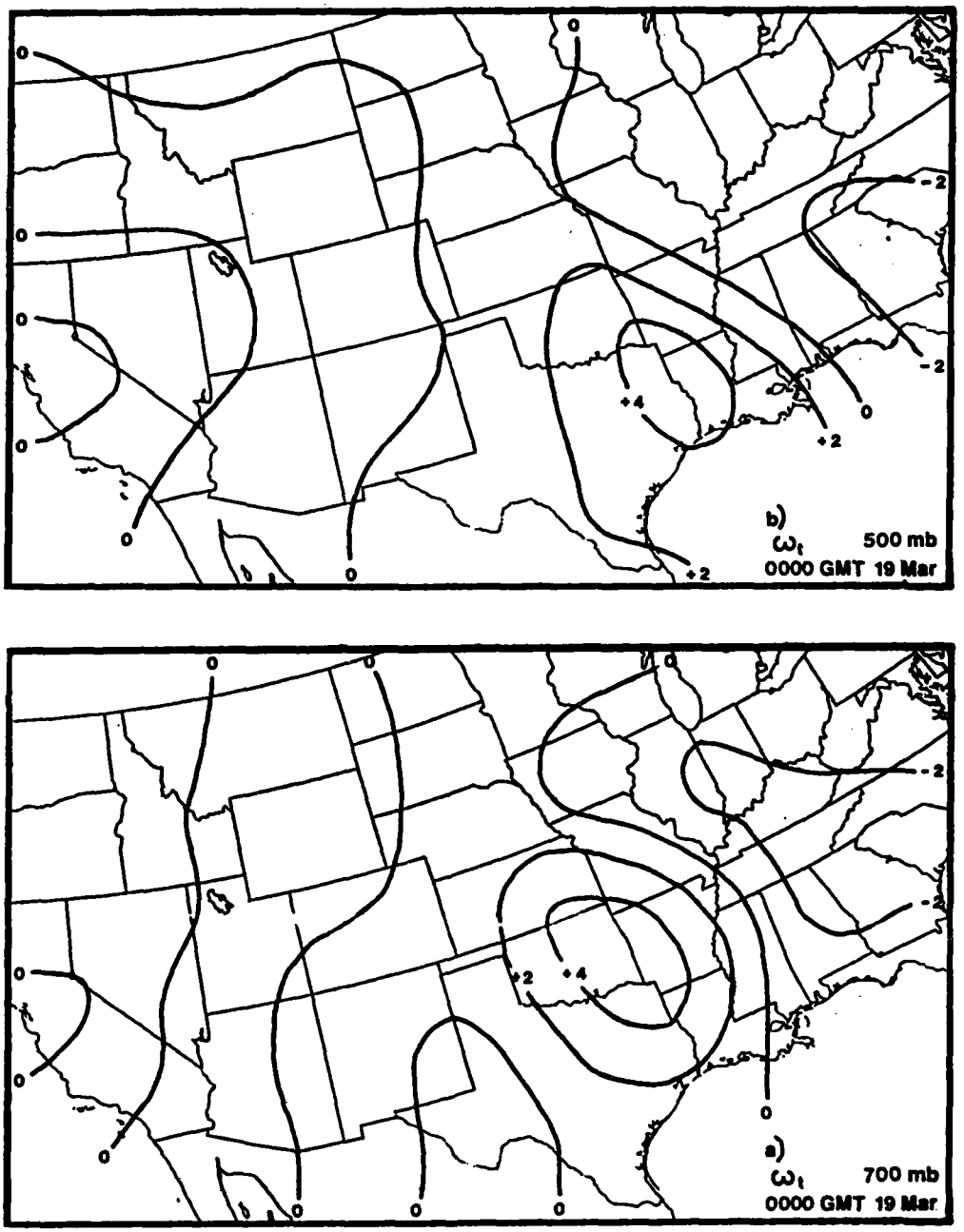

Fig. 22 As in Fig. 19, but for 0000 GMT 19 March 1986.

not indicative of the thunderstorms which occurred ahead of the front. On the other hand, this method does outperform the traditional technique by extending the rising motion over northern Montana where precipitation was present. The 500 mb field (Fig. 22b) is similar to that from the traditional routine (Fig. 14b) except over Arizona, New Mexico, and southern California where Trenberth's method produces upward motion and over the southeastern United States where Trenberth's scheme yields weaker ascent.

From a subjective perspective, results from Trenberth's procedure are very comparable to those from the traditional omega equation. The differences that were noted were relatively minor. Generally, the fields produced by these two methods did not correlate as well with the cloud and precipitation areas as did the kinematic variety.

The final method to be analyzed involves the divergence of Q vectors. Based on the limitations of the previous two methods, the Q vector procedure outlined by Hoskins et al. (1978) was expected to produce the best results. The 700 mb ω field at 1200 GMT 17 March (Fig. 23a) is similar to those from the previous two omega equations (Figs. 11a and 19a). There is weak rising motion ahead of the cold front (Fig. 2) and weak subsidence behind it. However, the Q vector approach is

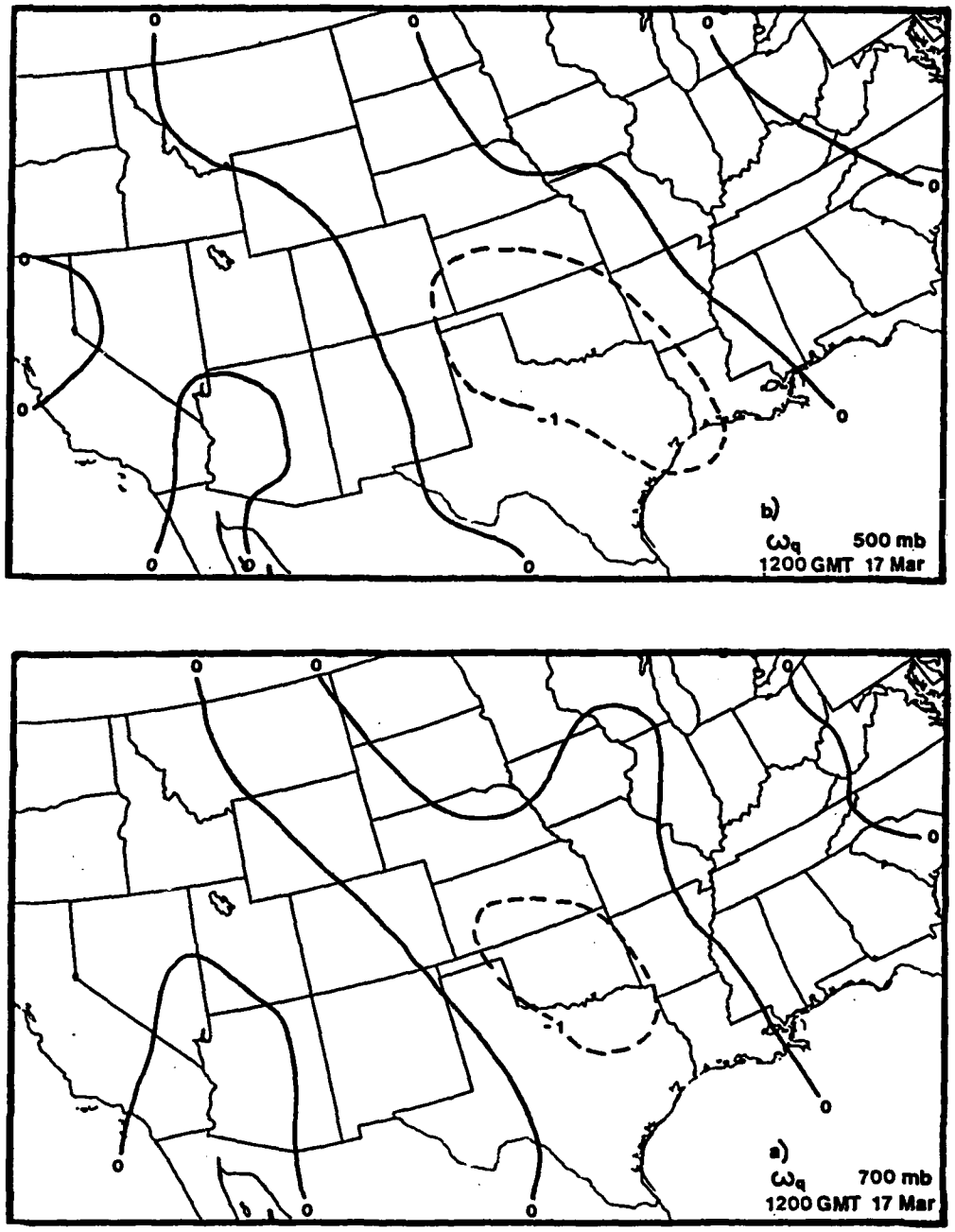

Fig. 23 Vertical motions (microbars/s) from the Q vector form of the omega equation at a) 700 mb and b) 500 mb for 1200 GMT 17 March 1986.

the only procedure that yields rising motion near the thunderstorms over San Diego, CA. At 500 mb (Fig. 23b), the field also is very similar to Trenberth's variety (Fig. 19b), with the rising motion over Arizona corresponding to showers there.

Figure 24a shows 700 mb Q vector vertical motions at 0000 GMT 18 March. Values of the ascent/descent couplet are smaller than those from the other methods, but the placement of features is very similar to that from the traditional (Fig. 12a) and Trenberth schemes (Fig. 20a). Upward motion is located ahead of the cyclone (Fig. 3) with subsidence behind the cold front. The biggest difference occurs at 500 mb (Fig. 24b). Here, the Q vector approach produces rising motion over northeastern Montana and northern Arizona. Both of these precipitation areas were in regions of subsidence according to the other two routines (Figs. 12b and 20b).

The 700 mb vertical motion field at 1200 GMT 18 March (Fig. 25a) also is similar to those from the previous two omega equation formulations (Figs. 13a and 21a) in that moderate upward motion is indicated ahead of the cyclone (Fig. 4). The biggest difference is in eastern Montana and western North Dakota where the Q vector procedure does better than the other methods because it produces rising motion in this precipitation region. At 500 mb (Fig. 25b), the Q vector vertical motions away from the cyclone

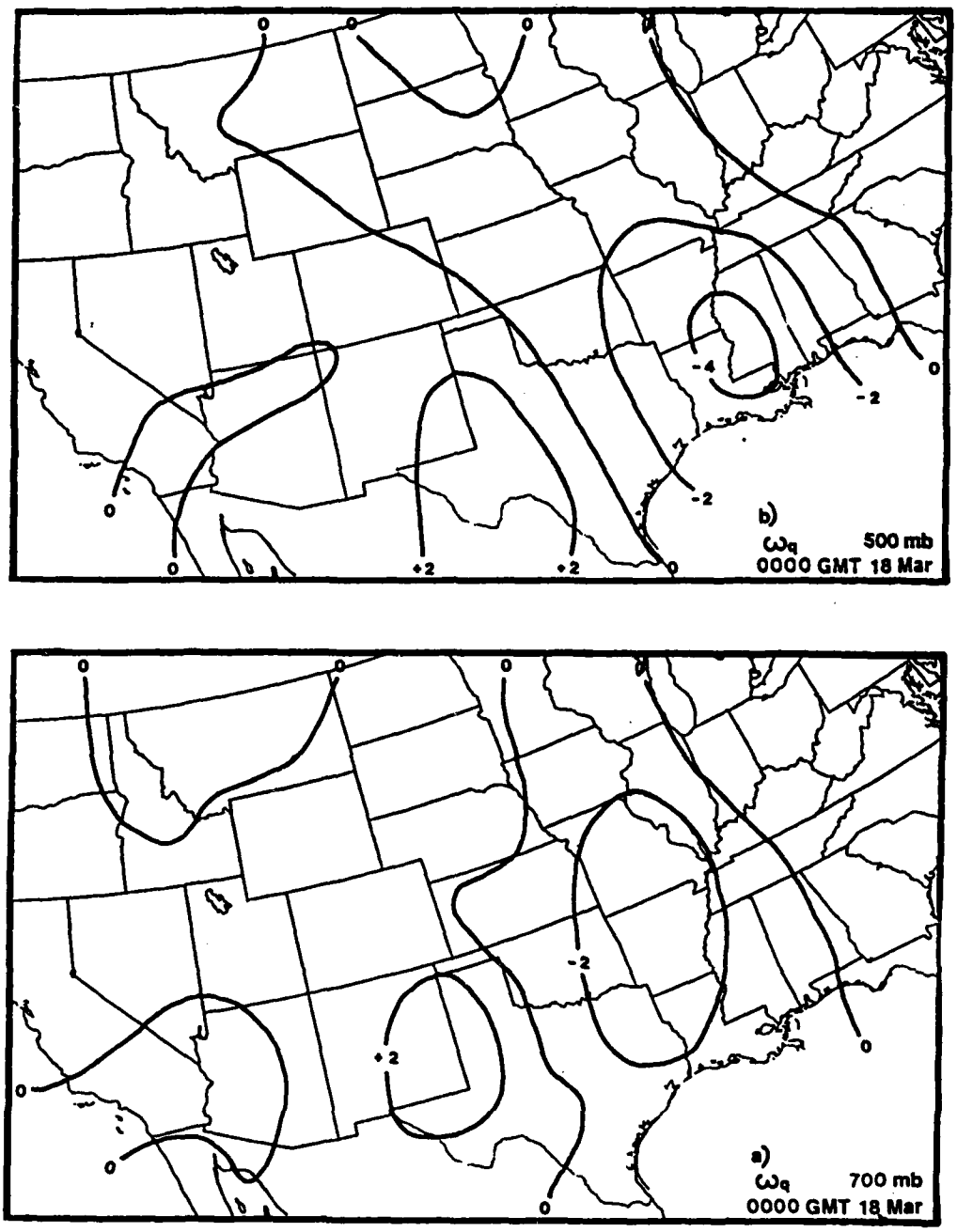

Fig. 24 As in Fig. 23, but for 0000 GMT 18 March 1986.

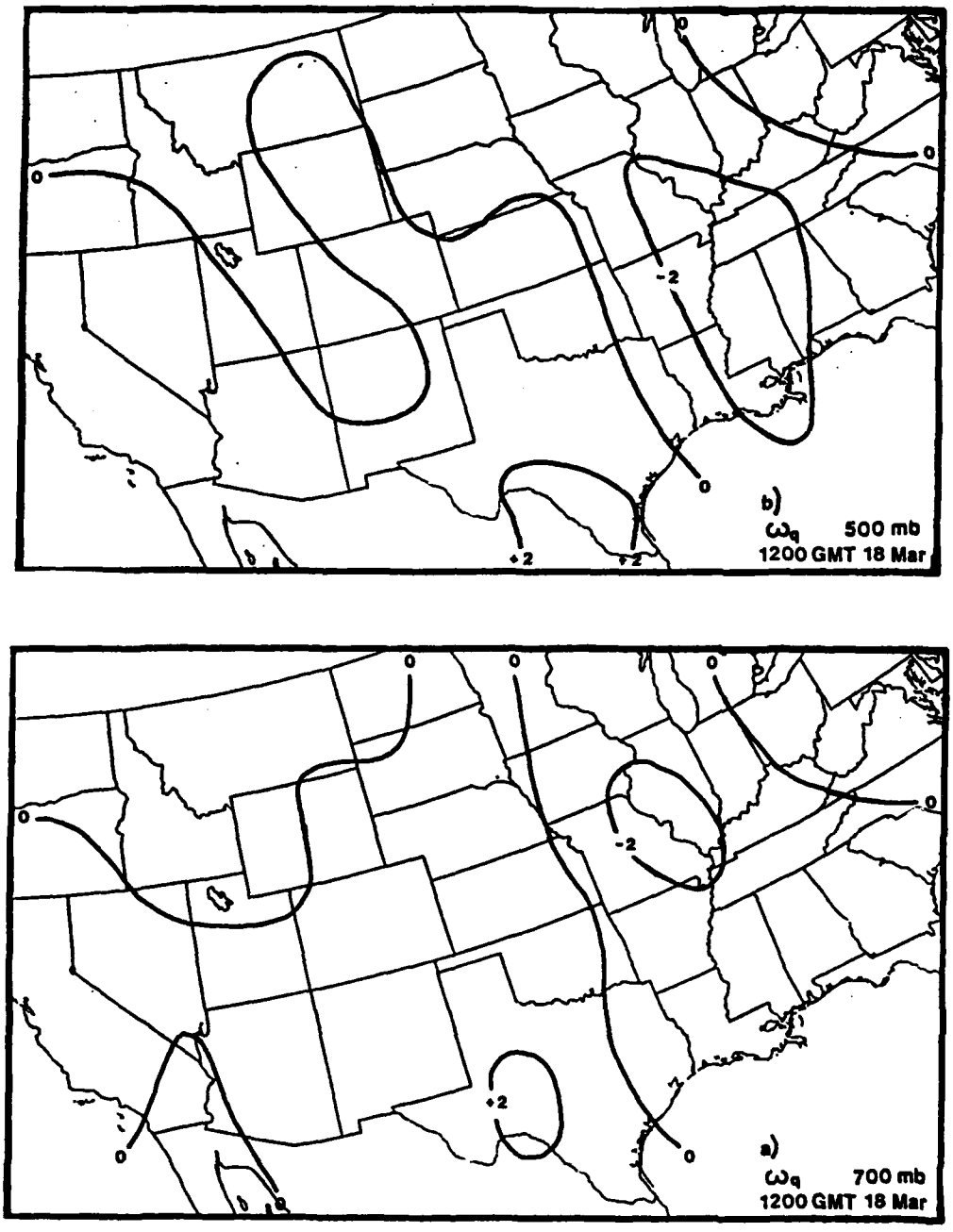

Fig. 25 As in Fig. 23, but for 1200 GMT 18 March 1986.

center are better aligned with the precipitation regions than those from the other two algorithms (Figs. 13b and 21b).

Finally, the 700 mb ω field at 0000 GMT 19 March (Fig. 26a) once again closely resembles Trenberth's variety (Fig. 22a), with rising motion ahead of the cold front and 500 mb trough (Fig. 5) and subsidence behind it. In addition, both methods outperform the traditional scheme (Fig. 14a) in northern Montana by producing rising motion that corresponds to the snow. The 500 mb ω field (Fig. 26b) is also similar to that from Trenberth's formulation (Fig. 22b). Again, both approaches do better than the traditional method (Fig. 14b) as far as precipitation areas are concerned.

As described earlier, the divergence of Q vectors is the forcing function for this technique. In general, Q vector convergence at a given level indicates regions of upward vertical motion; that is, the Q vectors at that level will point to the rising motion. Durran and Snellman (1987), Barnes (1985), and others have stated that Q vectors at individual pressure levels can be used to infer vertical motion. In the current case, this point is illustrated by comparing 700 mb Q vectors (Fig. 27) at 0000 GMT 18 March with the corresponding 700 mb vertical motion field (Fig. 24a). Notice how the Q vectors in the Midwest converge ahead of the cyclone (Fig. 3) in associ-

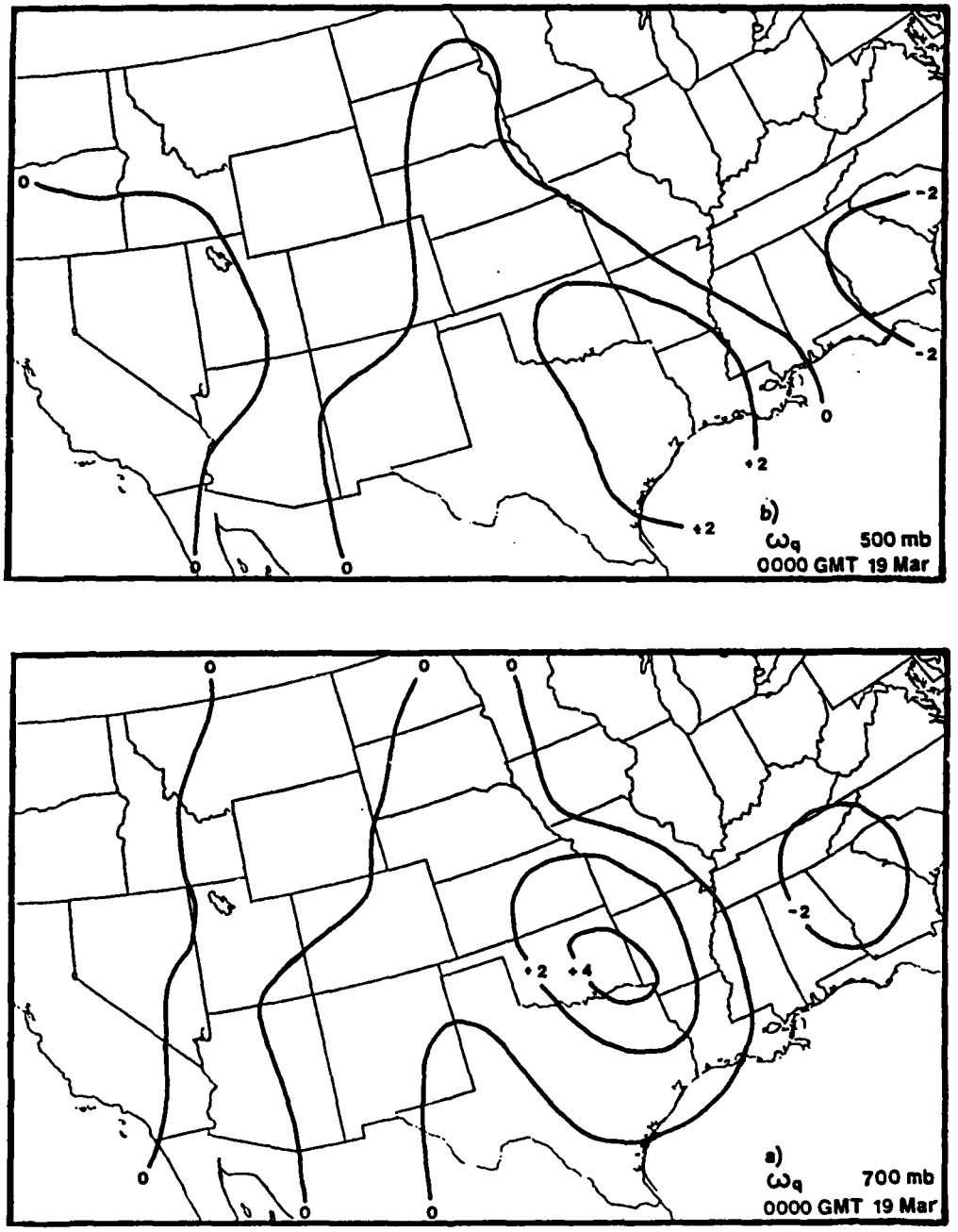

Fig. 26 As in Fig. 23, but for 0000 GMT 19 March 1986.

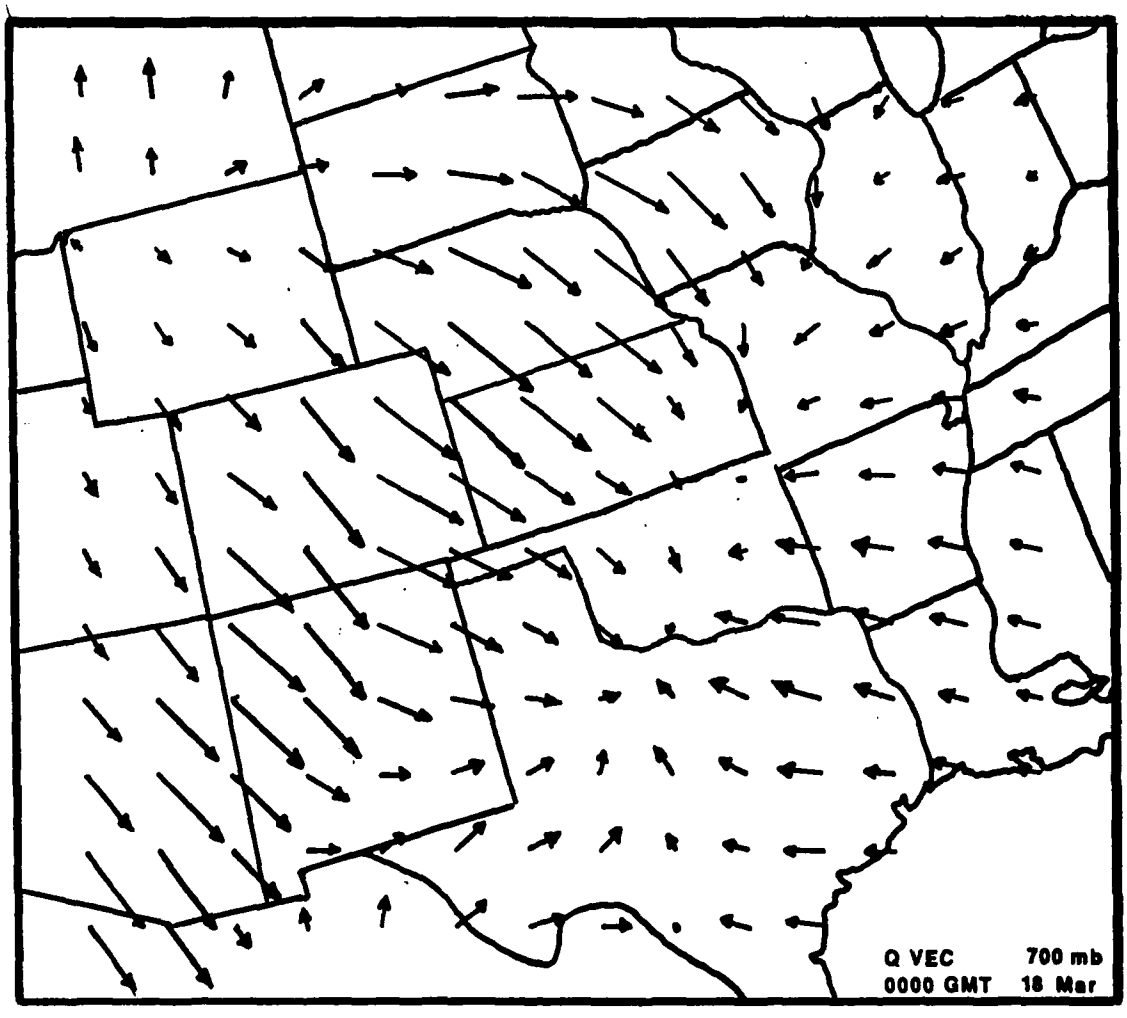

Fig. 27 Q vectors at 700 mb for 0000 GMT 18 March 1986.

ation with the rising motion. On the other hand, the subsidence over the Texas-New Mexico border is not obvious in the Q vector pattern.

To further analyze the relationship between Q vectors and vertical motion, Figs. 28a-d show Q vector divergence at 700 mb for the four times. Although rising (sinking) motion should correspond to Q vector convergence (divergence) at any given level, some displacement can be expected because the ω fields are obtained from three-dimensional relaxation. In general, the current divergence fields agree with the ω patterns; however, some discrepancies stand out. For example, notice the convergence over Iowa at 0000 GMT 18 March (Fig. 28b). This convergence is near the hailstorm which occurred 6 h earlier, but the upward motion (Fig. 24a) is located farther south. The most dramatic difference is at 0000 GMT 19 March (Figs. 28d and 26a). Convergence maxima over Iowa and Mississippi (Fig. 28d) are both over areas of intense thunderstorms during this time; however, the ω field (Fig. 26a) shows only weak upward motion in these areas. Furthermore, the convergence center over the Texas-Louisiana border corresponds to subsidence.

Durran and Snellman (1987) concluded that 700 mb may not be the best level for comparing Q vector forcing to the resulting vertical motion. The imposition of upper and lower boundary conditions and the vertical derivatives

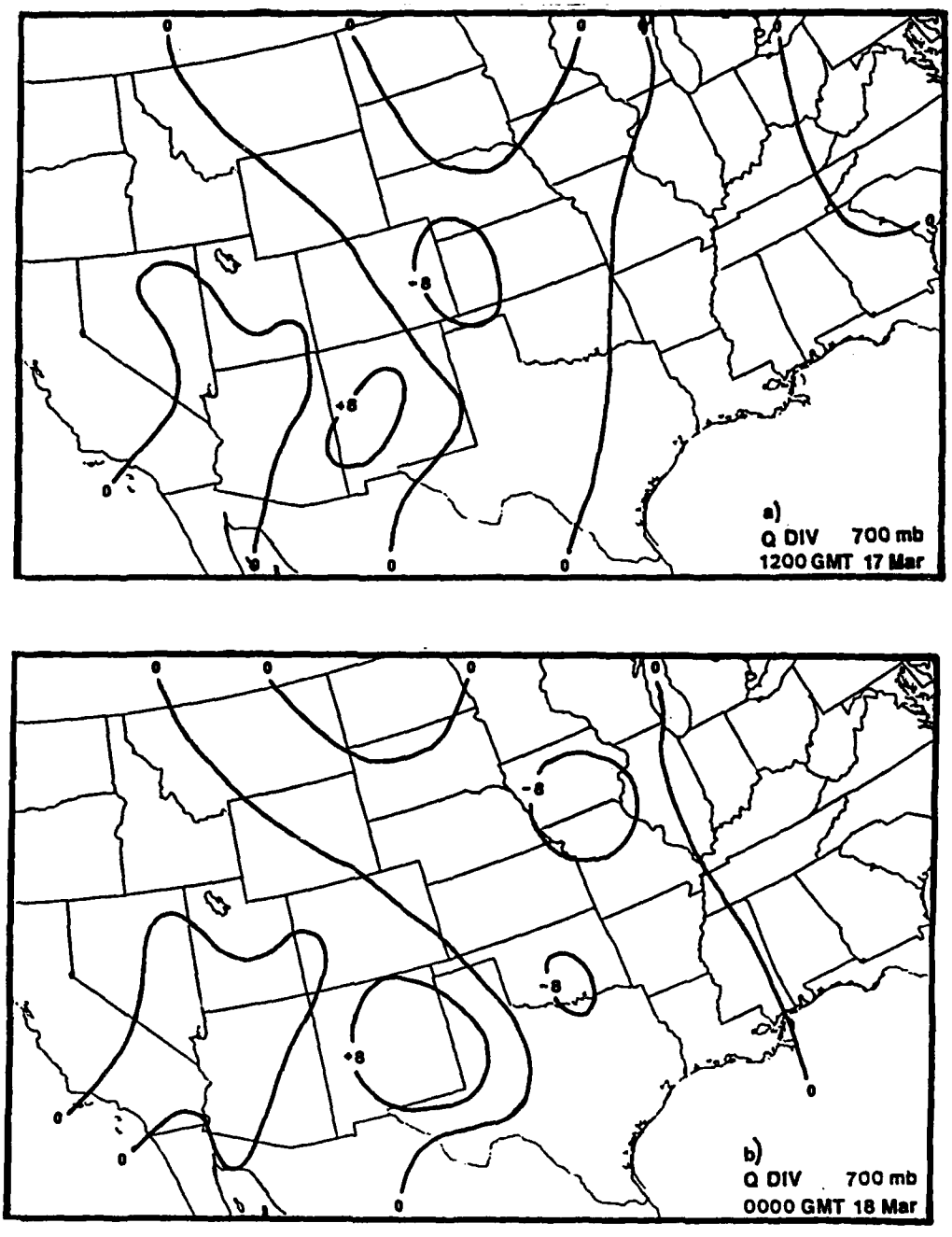

Fig. 28 Divergence of Q vectors (10^{-16} m/kg s) at 700 mb for a) 1200 GMT 17 March 1986, b) 0000 GMT 18 March 1986, c) 1200 GMT 18 March 1986, and d) 0000 GMT 19 March 1986.

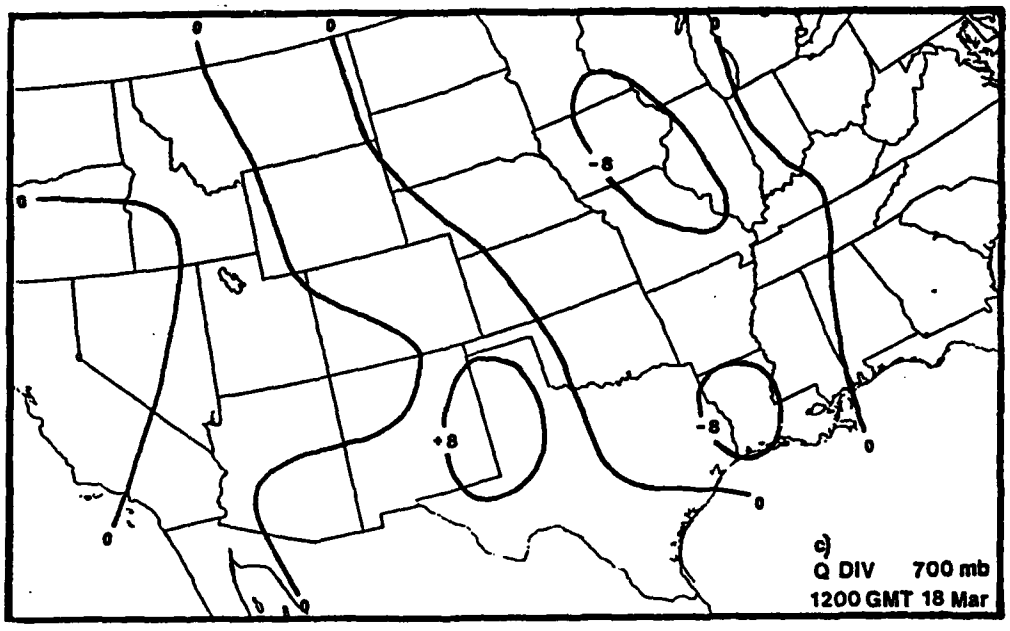

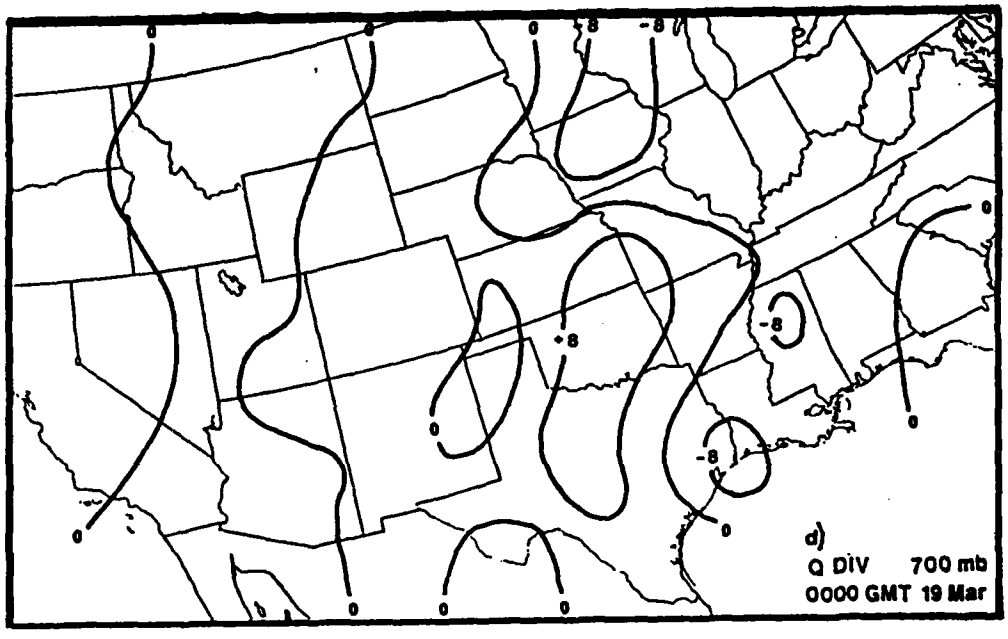

Fig. 28 (continued).

cause 700 mb vertical motions to be relatively insensitive to 700 mb forcing. Instead, they suggested that 700 mb motions should be related to 500 mb Q vector divergence. In the current case, values of 500 mb Q vector divergence (Figs. 29a-d) are greater in magnitude than those at 700 mb at all four times, and there are differences in patterns as well. However, Durran and Snellman (1987) stated that it is not uncommon for the 700 and 500 mb forcing to differ considerably. Once again, the 500 mb convergent areas usually agree with the regions of rising motion, but there still are exceptions. For example, at 0000 GMT 18 March (Fig. 29b), notice the strong convergence at 500 mb over the central Rockies, which was not seen in the 700 mb divergence field (Fig. 28b). Widespread precipitation was occurring over most of this area behind the surface low and at the base of the 500 mb trough (Fig. 3), even though both the 700 and 500 mb vertical motions (Fig. 24) exhibited subsidence. There also were large differences between the 500 mb Q vector divergence pattern (Fig. 29d) and the 500 mb vertical motions (Fig. 26b) at 0000 GMT 19 March. Specifically, the convergence maximum over eastern Texas is centered over subsidence as was the 700 mb convergence feature (Fig. 28d). Fortunately, however, the subsidence is over the clear area behind the surface cold front (Fig. 5). The important point here is that Q vectors and Q vector

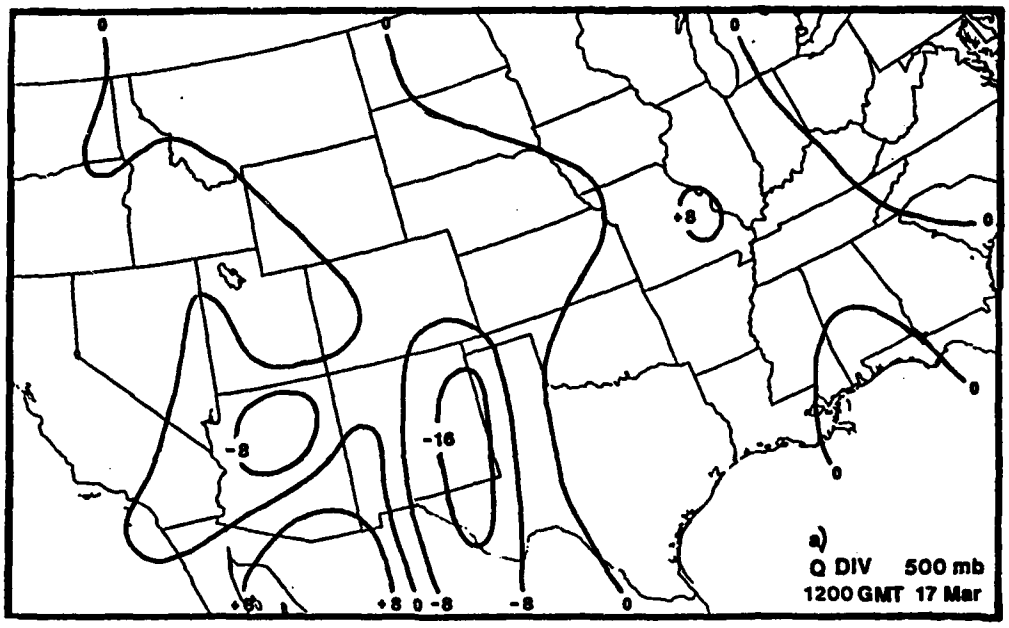

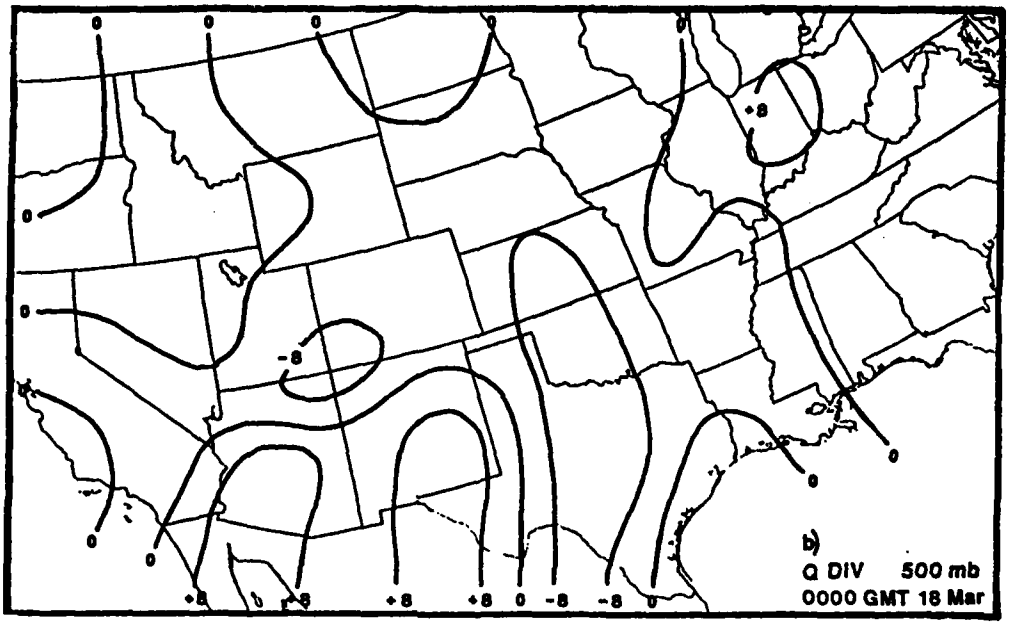

Fig. 29 As in Fig. 28, except for 500 mb.

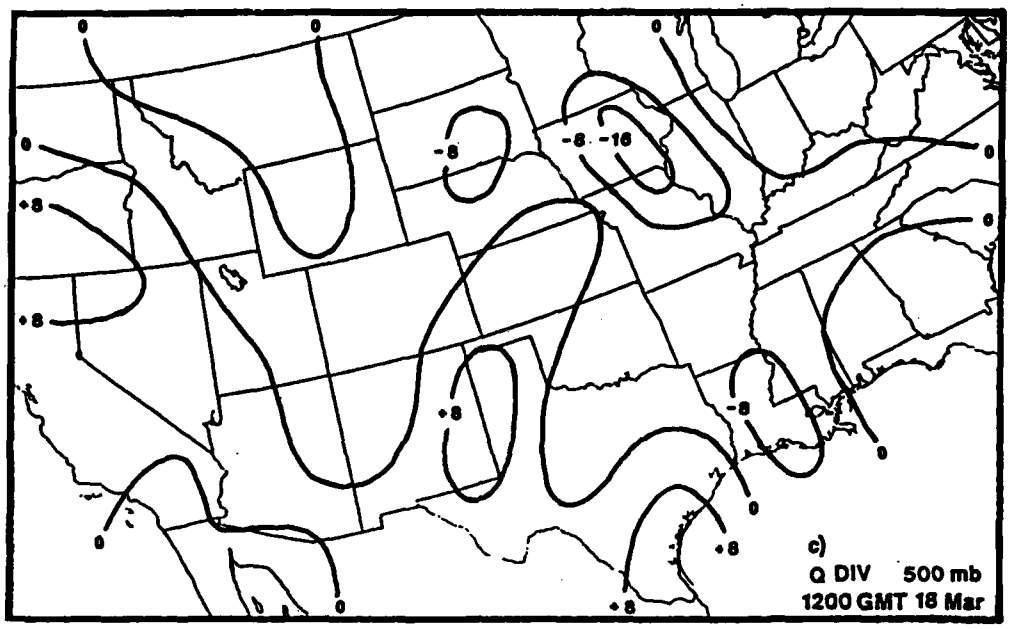

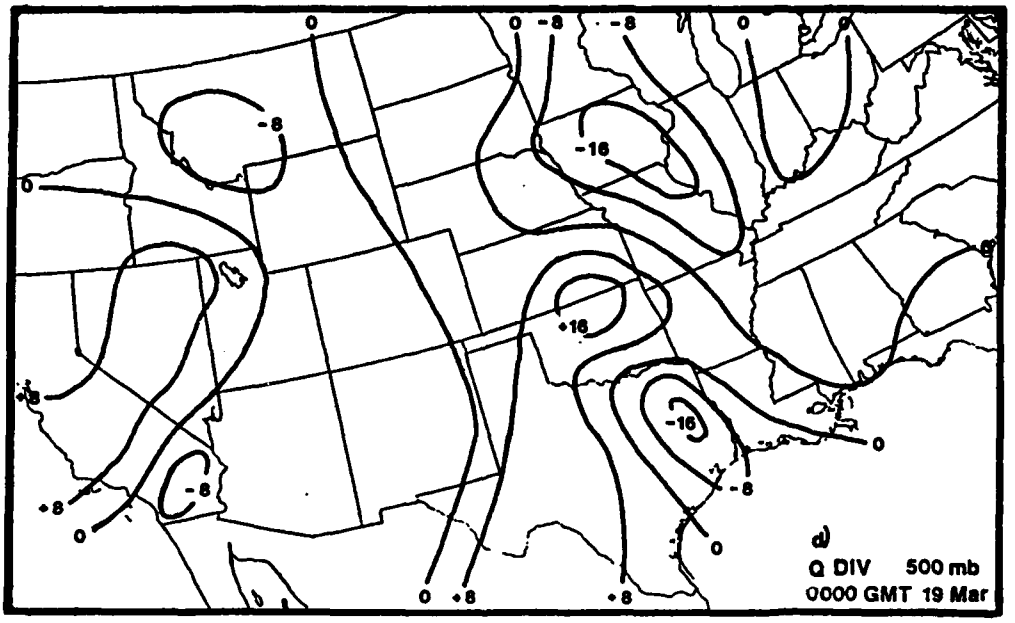

Fig. 29 (continued).

divergence at individual levels are not always indicative of the vertical motion. The previously cited studies, however, suggest that a closer agreement may be expected in many situations.

b. Objective comparisons

The subjective analyses clearly suggest that the kinematic vertical motions had the best correlation with the flow patterns and clouds/precipitation. However, the version of the omega equation having the most realistic results may not be obvious because the vertical motion fields were very similar in many cases. For this reason, an objective or quantitative scoring system was employed to help determine the best procedure.

The scoring scheme was developed by Smith and Lin (1978) and later used by Fuelberg and Lee (1982) in a similar comparison study. It is based on the previously mentioned assumption that ascent (descent) leads to clouds/precipitation (fair skies). Since the vertical motions were on a grid, the weather conditions also had to be gridded. Using the surface charts, each grid point was assigned a number based on the clouds and weather occurring at or near that grid point. The four following categories were used:

1) clear/scattered clouds (less than 5/10 coverage),

2) broken clouds (5/10 to 8/10 coverage),

3) overcast skies (greater than 8/10 coverage), and

4) radar echoes within one-half the grid spacing.

If a radar echo were present at any grid point, the cloud cover was ignored. Since the scoring was done at both 700 and 500 mb, categories were based on low clouds for 700 mb scoring, and low plus middle clouds for 500 mb scoring. As noted earlier, some of the observed features were at a smaller scale than permitted in the objectively analyzed data. Thus, these cloud features cannot be resolved by the vertical motions from any scheme. High clouds were not considered in the scoring since they were usually obscured by lower varieties and since vertical motions above 500 mb were considered less reliable than those below.

After the cloud data were gridded as described above, vertical motions at 700 and 500 mb were tabulated into the various categories at each grid point. Specifically, the values for each method were placed into 1.0 microbar/s intervals, a total of eight groups between 0 and $\pm$ 4 microbars/s for each weather category. This was done at each time separately, and all four times were added together to find the overall number of occurrences for the entire case study.

Once the number of occurrences was found, the methods were scored based on the following scheme:

1) For each 1 microbar/s upward motion interval, one point was given to the method which had the highest number of category 4 (precipitation) occurrences; another point was given to the method with the highest number of occurrences in categories 3+4 (cloud or precipitation).

2) For each 1 microbar/s downward motion interval, one point was given to the method which had the lowest number of category 4 occurrences; another point was given to the method with the lowest number of occurrences in categories 3+4.

3) Finally, the method having the largest percentage of upward motion in category 4 was given one point. Also, the method having the largest percentage of upward motion in categories 3+4 was given a point. Similarly, the method having the smallest percentage of upward motion in category 1 was given one point.

If any method had the same number of occurrences in a given category during the scoring, one point was given to each of the methods. To interpret the results, the vertical motions having the highest score best relate to the cloud/precipitation patterns.

Since stronger ascent (descent) should be more likely to produce clouds and precipitation (fair skies) than weaker motion, more emphasis should be placed on agreements between clouds/precipitation and the larger values of vertical motion. In order to do this, a weighted

scoring scheme outlined by Smith and Lin (1978) was used. Specifically, the first two steps of the scoring procedure were repeated using weights of 1, 1.5, 2, and 2.5 for each of the successively greater intervals on both the upward and downward motion side.

Before evaluating the scores, it is advantageous to consider frequency distributions of vertical motion for two of the weather categories (Fig. 30). The Trenberth form of vertical motions depicted here includes the deformation effect. Omission of deformation (not shown) produced a distribution almost identical to that presented. For each level and category, notice that the kinematic method produced a wider distribution of values. Also, curves of kinematic motions are the most realistic since they peak in the downward motions for category 1 (clear to scattered clouds) and in the upward motions for categories 3+4 (overcast or precipitating). Peaks for the three omega equation schemes are more narrow, centered in the 0.0 to 1.0 microbar/s interval in all four panels. Furthermore, in category 1 (Figs. 30a-b), the kinematic procedure has the most points (the greater area) on the downward motion side, thereby suggesting the best results. At 500 mb (Fig. 30b), the peak of the kinematic curve is well into the subsidence side, which also is much more realistic. In categories 3+4 (Figs. 30c-d), the kinematic method has the most

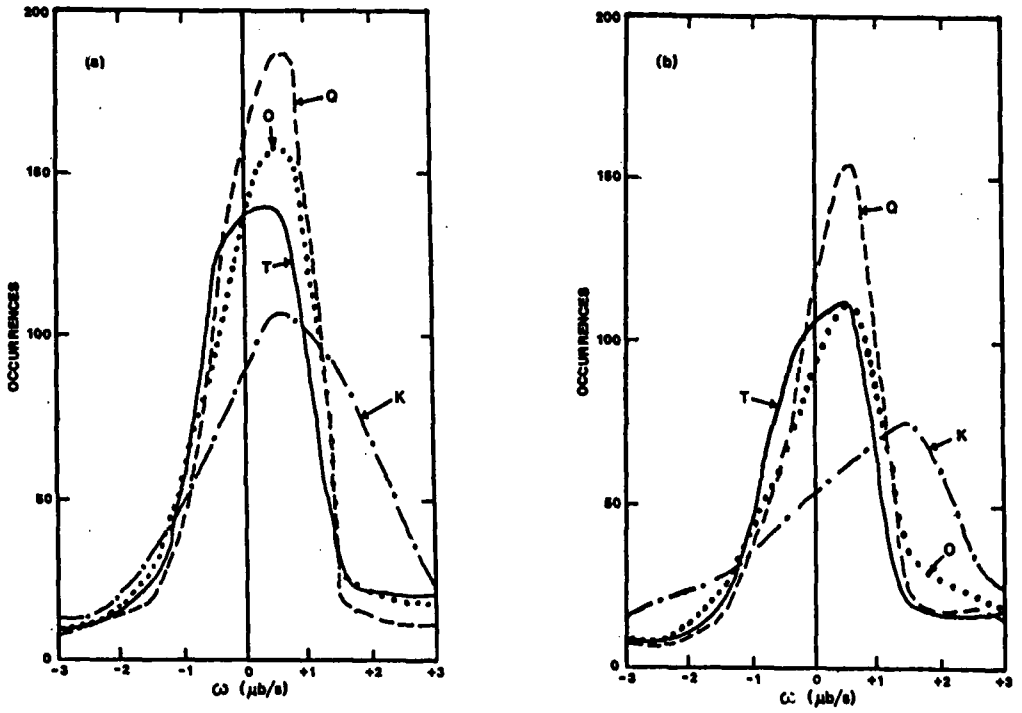

Fig. 30 Frequency distribution of vertical motion in 1 microbar/s intervals for the composite 48 h period. The panels are a) 700 mb for clear to scattered low or middle clouds (category 1), b) 500 mb for category 1, c) 700 mb for overcast low or middle clouds or precipitation (category 3+4), d) 500 mb for category 3+4. "K" denotes kinematic motions, "O" denotes the original form of the omega equation, "T" denotes Trenberth's form of the omega equation, and "Q" denotes the Q vector form of the omega equation.

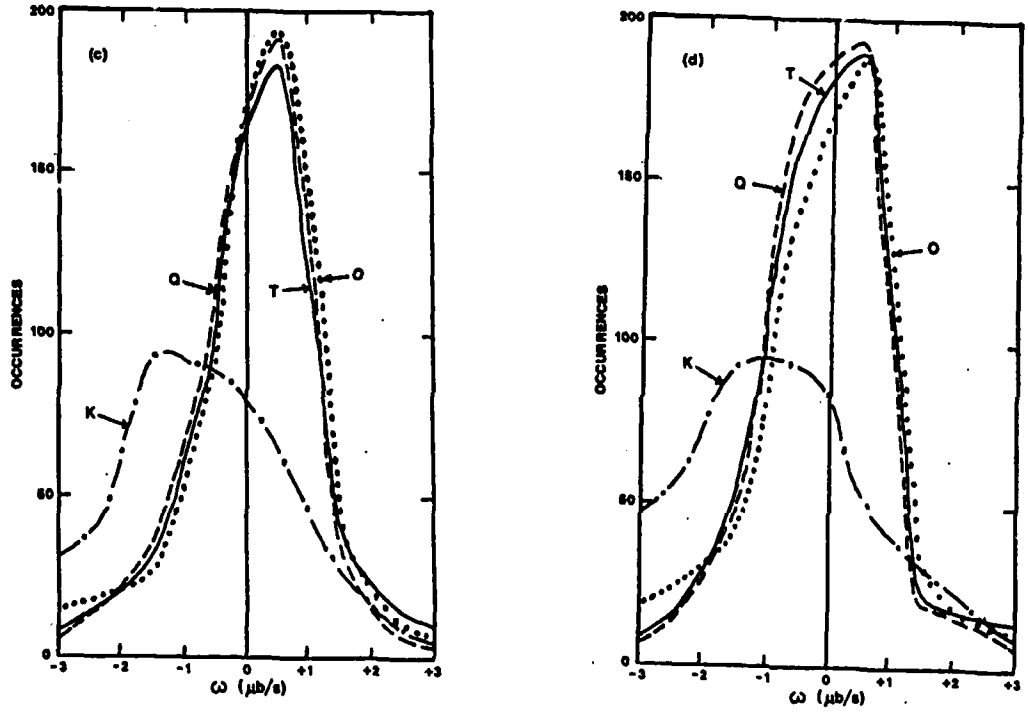

Fig. 30 (continued).

points with upward motion, as well as peaks centered in the ascent range. Curves for the omega equation formulations are very similar to each other, but unfortunately, their peaks are on the downward motion side.

Results of the scoring scheme are shown in Tables 1-5. Table 1 contains the non-weighted scores of each method at both 700 and 500 mb. At both the individual times as well as the composite, it is clear that the kinematic routine scores higher (better). The Q vector approach seems to be the next best; however, there is a major difference in score between these two. When the scoring scheme is repeated for only the omega equation methods, the results are much closer (Table 2). Each method fares differently at the individual times depending on the synoptic conditions; however, when looking at the composite of all four times, the Q vector approach receives the most points at both 700 and 500 mb. Notice the small difference between the Trenberth method with and without the deformation function, with slightly better performance without the function. There is no obvious explanation for this surprising result, and it may not be significant. Nonetheless, the similarity suggests that deformation can be safely omitted during this case.

As described earlier in this section, the scoring scheme was also done with weighted values. Table 3 shows

Table 1. Non-weighted scores for weather class/vertical motion occurrences at 700 mb and 500 mb. Values for individual and composite times are given. The scoring procedure is described in the text.

Method	17 Mar 1200 GMT	18 Mar 0000 GMT	18 Mar 1200 GMT	19 Mar 0000 GMT	All times
700 mb					
Kinematic	13	16	15	13	15
Traditional	8	3	2	0	0
Trenberth (with def.)	8	2	2	0	0
Trenberth (without def.)	8	0	2	3	0
Q Vector	10	3	8	5	4
500 mb					
Kinematic	9	14	14	10	12
Traditional	5	2	2	1	1
Trenberth (with def.)	6	1	2	4	1
Trenberth (without def.)	7	1	4	4	0
Q Vector	8	4	5	4	8

Table 2. As in Table 1, except for the omega equation methods only.

Method	17 Mar 1200 GMT	18 Mar 0000 GMT	18 Mar 1200 GMT	19 Mar 0000 GMT	All times
700 mb					
Traditional	11	8	5	4	3
Trenberth (with def.)	10	4	4	3	1
Trenberth (without def.)	12	6	8	6	5
Q Vector	16	7	11	10	11
500 mb					
Traditional	10	4	6	5	4
Trenberth (with def.)	11	2	4	8	1
Trenberth (without def.)	13	9	10	6	6
Q Vector	15	12	7	6	10

Table 3. As in Table 1, except for weighted scores.

Method	17 Mar 1200 GMT	18 Mar 0000 GMT	18 Mar 1200 GMT	19 Mar 0000 GMT	All times
700 mb					
Kinematic	22.0	27.0	24.5	23.0	25.0
Traditional	17.0	5.0	5.0	0.0	0.0
Trenberth (with def.)	17.0	3.0	5.0	0.0	0.0
Trenberth (without def.)	17.0	0.0	6.0	4.5	0.0
Q Vector	19.0	7.0	14.5	7.5	6.0
500 mb					
Kinematic	16.5	22.5	24.0	16.0	21.0
Traditional	10.0	4.0	5.0	2.0	2.0
Trenberth (with def.)	12.0	2.0	4.0	5.0	1.5
Trenberth (without def.)	13.5	2.0	6.5	5.5	0.0
Q Vector	14.0	6.5	9.0	6.0	13.5

these results for all methods. Once again, the kinematic technique receives more points than any other approach, with the Q vector algorithm coming in a rather distant second. When considering only the omega equation methods (Table 4), the results are similar to the non-weighted variety (Table 2). Different routines have highest scores at individual times, but the Q vector approach exhibits the overall superiority at both 700 and 500 mb. There again is little difference between scores of the complete and simplified forms of Trenberth's procedure.

The last step in the scoring scheme compares the percentages of vertical motion in categories 1, 3+4, and 4. Table 5 shows the percentage of upward motion in each of these categories at 700 and 500 mb. In all cases, the kinematic method produces the highest percentage of upward motion in the cloud and precipitation categories (3+4 and 4), but does not always have the lowest percentage in category 1. Among the omega equations, the Q vector scheme has the lowest percentage of upward motion in category 1 and the highest percentage in both categories 3+4 and 4 in the composite column.

To summarize the scoring results, the kinematic method was found to be clearly superior. However, when comparing the four omega equation techniques by themselves, the Q vector approach fared the best when the composite of times was considered. At the individual

Table 4. As in Table 2, except for weighted scores.

Method	17 Mar 1200 GMT	18 Mar 0000 GMT	18 Mar 1200 GMT	19 Mar 0000 GMT	All times
700 mb					
Traditional	16.0	9.0	11.5	10.0	6.5
Trenberth (with def.)	15.0	6.5	8.5	5.5	2.0
Trenberth (without def.)	18.0	10.0	14.5	9.5	6.0
Q Vector	20.0	16.0	18.0	15.5	17.0
500 mb					
Traditional	21.0	9.0	13.5	10.0	9.0
Trenberth (with def.)	22.0	4.5	7.5	9.0	1.5
Trenberth (without def.)	25.0	16.0	15.5	10.5	8.0
Q Vector	26.0	18.5	12.5	11.0	15.5

Table 5a. Percentage occurrence of upward motion for the individual weather classes at 700 mb. Values for individual and composite times are given.

Method	17 Mar 1200 GMT	18 Mar 0000 GMT	18 Mar 1200 GMT	19 Mar 0000 GMT	All times
Kinematic					
Cat. 1	32%	34%	44%	26%	35%
Cat. 3+4	78%	81%	83%	67%	76%
Cat. 4	78%	78%	89%	70%	78%
Traditional					
Cat. 1	37%	42%	51%	23%	39%
Cat. 3+4	40%	39%	37%	39%	39%
Cat. 4	37%	33%	29%	43%	36%
Trenberth (with def.)					
Cat. 1	42%	44%	58%	33%	45%
Cat. 3+4	44%	38%	33%	41%	39%
Cat. 4	45%	32%	29%	44%	38%
Trenberth (without def.)					
Cat. 1	39%	43%	53%	19%	40%
Cat. 3+4	44%	36%	33%	41%	38%
Cat. 4	38%	33%	37%	46%	39%
Q Vector					
Cat. 1	38%	45%	35%	30%	37%
Cat. 3+4	48%	36%	38%	44%	41%
Cat. 4	49%	30%	32%	49%	39%

Table 5b. As in Table 5a, except for 500 mb.

Method	17 Mar 1200 GMT	18 Mar 0000 GMT	18 Mar 1200 GMT	19 Mar 0000 GMT	All times
Kinematic					
Cat. 1	42%	24%	43%	28%	36%
Cat. 3+4	73%	89%	84%	64%	78%
Cat. 4	73%	88%	89%	71%	80%
Traditional					
Cat. 1	40%	58%	43%	10%	37%
Cat. 3+4	54%	39%	52%	46%	47%
Cat. 4	38%	33%	47%	53%	43%
Trenberth (with def.)					
Cat. 1	34%	46%	58%	29%	42%
Cat. 3+4	46%	39%	54%	54%	48%
Cat. 4	38%	36%	50%	61%	47%
Trenberth (without def.)					
Cat. 1	40%	53%	52%	26%	43%
Cat. 3+4	54%	44%	59%	50%	51%
Cat. 4	41%	42%	63%	58%	51%
Q Vector					
Cat. 1	38%	40%	32%	16%	32%
Cat. 3+4	54%	45%	53%	51%	51%
Cat. 4	49%	42%	62%	61%	53%

times, no single omega equation procedure consistently had the higher point values. Thus, it is difficult to distinguish which of the omega equation schemes was superior.

5. Conclusions

The purpose of this paper was to objectively determine whether the kinematic method, the traditional quasi-geostrophic omega equation, Trenberth's form of the omega equation, or the Q vector form of the omega equation produced the most realistic synoptic scale vertical motions when compared to flow patterns and cloud/precipitation regions associated with a developing midlatitude springtime cyclone. To make this determination, the results from the techniques were subjectively analyzed and objectively tested using a scoring scheme.

The kinematic approach proved to be superior to the other methods. This is consistent with findings of others who have evaluated the scheme (e.g., Smith and Lin, 1978). The reasons for this superiority are not fully known. However, one possibility involves latent heat release. In the kinematic procedure, the winds may have responded to the considerable heating produced by the precipitation. On the other hand, the heating effect may not be as apparent in the geostrophic winds that are input to the quasi-geostrophic formulations. These equations do not contain an explicit heating function.

When comparing only the results from the omega

equation algorithms, none of these versions were clearly superior. Since the omega equation procedures are, for the most part, simply different forms of each other, similar results should be expected. The formulations do differ, however, in their finite differencing, thereby accounting for the somewhat contrasting results. It was interesting that omission of deformation had very little affect on the Trenberth type of vertical motions. In fact, omission produced slightly superior results, although this may not be significant.

Since results of the omega equations were so similar, the merit of each method should then be determined by its ease of use. Durran and Snellman (1987) concluded that the technique of examining vorticity advection by the thermal wind, developed by Trenberth (1978) and Sutcliffe (1947), was the simplest way of making a mental estimate of large scale vertical motion. On the other hand, they advocated the Q vector approach (Hoskins et al., 1978) when numerical computations were possible. Barnes (1985) suggested that Q vector divergence data be distributed to operational forecasters by the National Meteorological Center. This would allow easy visualization of vertical motions at a given level. Their ease of interpretation, ease of accurate calculations, and objective scoring superiority during the current case lead this author to conclude that Q vector vertical motions are superior to

those from the other omega equation methods.

REFERENCES

Bannon, J.K., 1948: The estimation of large-scale vertical currents from the rate of rainfall. Quart. J. R. Meteor. Soc., 74, 57-66.

Barnes, S.L., 1973: Mesoscale objective analysis using weighted time-series observations. NOAA Tech. Memo. ERL NSSL-62, National Severe Storms Laboratory, Norman, OK 73069, 60 pp. [NTIS COM-73-10781.]

----------, 1985: Omega diagnostics as a supplement to LFM/MOS guidance in weakly forced convective situations. Mon. Wea. Rev., 113, 2122-2141.

----------, 1986: On the accuracy of omega diagnostic computations. Mon. Wea. Rev., 114, 1664-1680.

Bellamy, J.C., 1949: Objective calculations of divergence, vertical velocity and vorticity. Bull. Amer. Meteor. Soc., 30, 45-49.

Belt, C.L., and H.E. Fuelberg, 1982: The effects of random errors in rawinsonde data on derived kinematic quantities. Mon. Wea. Rev., 110, 91-101.

Blakley, P.D., R.C. Molinaro, and J.T. Moore, 1986: A comparison of synoptic scale vertical motion calculations for the 30-31 January 1982 midwest snowstorm. Preprints, Eleventh Conf. Weather Forecasting and Analysis, Kansas City, Amer. Meteor. Soc., 78-82.

Durran, D.R., and L.W. Snellman, 1987: The diagnosis of synoptic-scale vertical motion in an operational environment. Weather and Forecasting, 2, 17-31.

Dutton, J.A., 1976: The Ceaseless Wind: An Introduction to the Theory of Atmospheric Motion. McGraw Hill, New York, 579 pp.

Fuelberg, H.E., and T.W. Funk, 1987: Diagnosis of vertical motion from VAS retrievals. J. Climate Appl. Meteor., 26, 1655-1670.

----------, and W.S. Lee, 1982: A comparison of ad-

iabatic and kinematic vertical motions using mesoscale data. Preprints Ninth Conf. Weather Forecasting and Analysis, Seattle, Amer. Meteor. Soc., 417-423.

Haltiner, G.J., and R.T. Williams, 1980: Numerical Prediction and Dynamic Meteorology (second edition). John Wiley and Sons, New York, 477 pp.

Holton, J.R., 1979: An Introduction to Dynamic Meteorology (second edition). Academic Press, New York, 391 pp.

Hoskins, B.J., I. Draghici, and H.C. Davies, 1978: A new look at the ω equation. Quart. J. Roy. Meteor. Soc., 104, 31-38.

----------, and M.A. Pedder, 1980: The diagnosis of middle latitude synoptic development. Quart. J. Roy. Meteor. Soc., 106, 707-719.

Miller, A., and H.A. Panofsky, 1958: Large-scale vertical motions and weather in January 1953. Bull. Amer. Meteor. Soc., 39, 8-13.

O'Brien, J.J., 1970: Alternate solution to the classical vertical velocity problem. J. Appl. Meteor., 9, 197-203.

Panofsky, H.A., 1946: Methods of computing vertical motion in the atmosphere. J. Meteor., 3, 45-49.

Portis, D.H., and P.J. Lamb, 1988: Estimation of large-scale vertical motion over the central United States for summer. Mon. Wea. Rev., 116, 622-635.

Smith, P.J., 1971: An analysis of kinematic vertical motions. Mon. Wea. Rev., 99, 715-724.

----------, and C.P. Lin, 1978: A comparison of synoptic-scale vertical motions computed by the kinematic method and two forms of the omega equation. Mon. Wea. Rev., 106, 1687-1694.

Sutcliffe, R.C., 1947: A contribution to the problem of development. Quart. J. Roy. Meteor. Soc., 73, 370-383.

Trenberth, K.E., 1978: On the interpretation of the diagnostic quasi-geostrophic omega equation. Mon. Wea.

Rev., 106, 131-137.

Vincent, D.G., K.E. Bossingham, and H.J. Edmon,Jr., 1976: Comparison of large scale vertical motions computed by the kinematic method and quasi-geostrophic ω equation. Preprints Sixth Conf. Weather Forecasting and Analysis, Albany, Amer. Meteor. Soc., 357-364.

Wilson, G.S., 1976: Large-scale vertical motion calculations in the AVE-IV Experiment. Geophys. Res. Lett., 3, 735-738.